Fermilab Proposal No. 669
Scientific Spokesman:

Brad Cox
Fermilab

FTS No: 312-370-3152
Commercial No:
312-840-3152

E-537 PHASE II

REVISED OBJECTIVES

(Updated January 1981)

A Comparison of the Production of Direct Photons and Resonances Decaying to Lepton Pairs by Antiproton/π^- and Proton/π^+ Beams

M. Binkley, B. Cox, J. Enagonio, C. Hojvat, D. Judd, R. Kephart, P. Mazur, C. T. Murphy, F. Turkot, R. Wagner, D. Wagoner, W. Yang
Fermi National Accelerator Laboratory

E. Anassontzis, P. Karabarbounis, S. Katsanevas, P. Kostarakis, C. Kourkoumelis, A. Markou, L. Resvanis, G. Voulgaris
University of Athens

H. Areti, S. Conetti, P. Lebrun, D. Ryan, D. Stairs
Mc Gill University

He Mao, Zhang Nai-jian
Shandong University
Peoples Republic of China

DIRECTOR'S OFFICE
JAN 23 1981

Table of Contents

Abstract

I Physics Goals
- (a) Direct photons
- (b) Heavy quark resonances with dilepton decay signature

II Beams

III Apparatus

IV Direct Photons
- (a) Event rates
- (b) Backgrounds
- (c) Trigger rates

V Resonance Study
- (a) Event rates/Backgrounds
- (b) Trigger rates

References

Appendix A - Liquid Argon Detector

Appendix B - Cerenkov Counters

Appendix C - Current Results from E-537

ABSTRACT

The special high intensity beams available at the highest secondary beam energies and the large aperture spectrometer of E-537 (see Appendix C) in the High Intensity Laboratory of the Proton Area present a unique place in which to search for and study phenomena associated with the production of direct photons and lepton pairs. We are updating our objective and restating[1] our intent to continue the experimentation begun in E-537 - Phase I with a comparison of direct photon production by both negative and positive beams

$$\begin{pmatrix} p^{\pm} \\ \pi^{\pm} \end{pmatrix} + N \rightarrow \gamma + X$$

and simultaneously to accumulate data of the type

$$\begin{pmatrix} p^{\pm} \\ \pi^{\pm} \end{pmatrix} + N \rightarrow \begin{pmatrix} \psi \\ \Upsilon \end{pmatrix} + \text{associated photons and charged particles}$$

to study heavy quark resonance formation and decay into final states containing a ψ or Υ.

A 1500 hour experiment at the highest available energies with the E-537 apparatus will allow us, because of the large cross sections, to measure and compare direct photon production by π^+, π^-, protons and antiprotons (an antiproton measurement is unique to this experiment) with good statistics out to $X_\perp \rightarrow 0.8$ over the entire range $X_F > 0$. With this data we will study the direct photon process itself and extract structure functions. In addition we will study the particles accompanying the photons for evidence of gluon and quark jet structure.

During this running the $(10^4 - 10^6)\psi$ and $(10^2 - 10^3)\Upsilon$ events accumulated will allow a study of heavy quark hadroproduction by both positive and negative beams. We will continue with greater

sensitivity the study of χ_ψ production begun by other experiments and at the higher energies make the first measurement of χ_Υ hadroproduction. Searches for beauty production will be made by looking for evidence of $B \to K\chi$, $K\pi\chi$, and $K\psi$, $K\pi\psi$.

I. Physics Goals - With the photon and lepton pair resonance data which can be accumulated in a total of 1500 hours of data taking with one of the beam scenarios described in Section II, the following studies will be undertaken:

a. Measurement of direct photon production

The direct production of photons at high $p_\perp$ in hadronic interactions[6-10] which has been observed at Fermilab and CERN[2-5] is thought to proceed in lowest order in α_s via the interactions of the constituent quarks and gluons shown in the following diagrams:

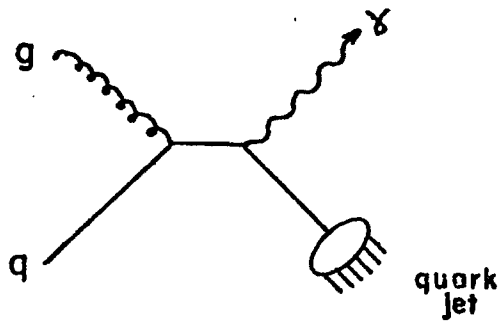

COMPTON

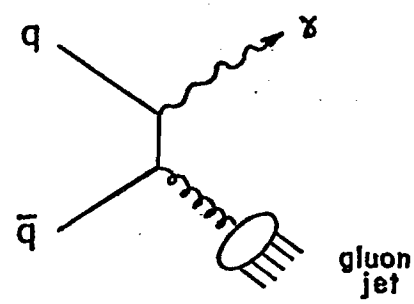

ANNIHILATION

In lepton pair production the virtual photon has mass M and materializes as a lepton pair, while in direct photon production the photon is on the mass shell. In the Compton process the direct photon recoils against a quark jet, and in the annihilation process the photon recoils against a gluon jet. The sum of the Compton and annihilation processes as calculated in QCD is thought to represent a good approximation to the production of direct photons at high $p_\perp$ if the quark and gluon structure functions include scale breaking effects. The production of direct photons by protons or π^+ in this picture will be dominated by the Compton process since the annihilation process proceeds mainly via valence antiquarks. The antiproton and π^-

interactions will have approximately equal contributions from the Compton and annihilation processes at moderate $p_\perp$, but at higher $p_\perp$ the annihilation process will dominate. By measuring the difference of the antiproton and proton cross sections from an isoscalar target such as D_2 we will isolate the annihilation process and make possible the construction of distributions which should show evidence of gluon jets. The same statement holds for the difference between the π^-D and π^+D cross sections except that in this case we are dealing with the pion gluon and quark distributions which are not as well understood as those of the proton or antiproton.

Our goals in the direct photon measurement are to run an equal amount of time with negative ($\bar{p}/\pi^-$) and positive (p/π^+) beams incident on an isoscalar D_2 target and to study the following direct photon cross sections over a large range of $X_\perp$ and X_F for the reasons indicated:

1. $\sigma_\gamma(\bar{p}D) - \sigma_\gamma(pD)$ — study of the annihilation process for nucleon valence quarks, for higher statistics extraction of the nucleon structure functions, and for extraction of information about gluon jets.

   $\sigma_\gamma(\pi^-D) - \sigma_\gamma(\pi^+D)$ — for the same reasons, except that the pion structure functions are studied in this data.

2. $\sigma_\gamma(pD)$ — to study the Compton process, to study the nucleon glue distribution, and to study quark jets.

   $\sigma_\gamma(\pi^+D)$ — study of the Compton process and to study the pion glue distribution. This process is complicated by a 25% admixture of the annihilation process.

3. $\sigma_\gamma(\bar{p}D)$ comparison of the antiproton production of direct photons themselves with the antiproton production of dimuons (which is being measured in E-537 Phase I) by comparison of the extracted structure functions.

b. Study of Heavy Quark Resonances

The accumulation of events with lepton pairs and photons in the final state will allow us to search for and study the hadroproduction and decay of heavy quark resonance states. In particular, with the mass resolution of our spectrometer, we should be able to resolve and to study charmonium 2^3P_J states with better statistics than has been achieved in any previous experiment.[11-15] We will test the predictions of the gluon fusion model[16-17] for these states and we will continue the search for evidence for the 2^1P_1 state. In addition, the higher energy beam scenarios which are available in the High Intensity Laboratory should make hadroproduction of the upsilonium spectrum experimentally accessible. We plan to search for and measure the $\chi_\Upsilon \to \gamma\Upsilon$ decays and to compare features of their production and decay with those of the χ_ψ. In every case the comparison of both positive and negative beams (and in particular the proton-antiproton comparison) will yield information about the production mechanisms of heavy resonances.

Finally, the high statistical levels and the good mass resolution for the χ_ψ states will not only allow us to continue the search[18] for the expected decays[19] of beauty $B \to \psi K$ and $B \to \psi K\pi$, but also for the first time, for the similar decays $B \to \chi K$ and $B \to \chi K\pi$.

II. Beams

Since the energy of the Fermilab accelerator will be undergoing major changes in the next four years and since the maximum energy of the secondary beam which can be transported to the spectrometer at a particular point in time is unclear, we have considered three different scenarios, each containing 750 hours of positive beam and 750 hours of negative beam operation. The particular scenario which we will choose will depend on the accelerator/secondary beam configuration which exists at the time of the experiment.

In all cases we have taken 1×10^7 incident secondary beam particles per second as a limiting rate, both for our beam tagging system and for the E-537 spectrometer in the open geometry configuration shown in figure 1. This beam flux corresponds to a maximum interaction rate of 3.5×10^6 interactions/second, since we plan to use a 1-meter long D_2 target. Deuterium is chosen both for its I = 0 nature and in order to optimize the ratio of radiation length to interaction length in the target material. We show in figure 2 the positive and negative secondary beam yields[20] available with a 400 GeV/c accelerator and with the 1000 GeV/c Tevatron. We will use both the special $\bar{\Lambda}^0 \to \bar{p}$ beam[21] (hereafter referred to as the neutral beam) and the conventional secondary transport[22] (referred to as the charged beam). The three beam scenarios are given at the end of this section.

The existing beam tagging system utilizes two 70' long differential Cerenkov counters operating at $\theta_c \sim 6.5$ mrad. They work well up to a beam momentum of 150 GeV/c. At 300 GeV/c we would employ two 95' long threshold Cerenkov counters ($\theta_c = 3.1$ mrad with an average of four photoelectrons per counter). With the particle ratios shown

in the beam scenarios these Cerenkov counters will allow less than 1% π^- contamination of the antiproton flux at 300 GeV/c. At 750 GeV/c we will not use tagging, since the positive beam is 98% protons and the negative beam is 99% π^-.

Accelerator/ Secondary Beam Configuration	Hours	Spill	Yields per spill	Total Beam
I. 400 GeV Accelerator 300 GeV Secondary Beam Transport (Current machine configuration)				
a. 100 GeV negative-secondary beam (neutral configuration - $\bar{\Lambda}^0 \to \bar{p}$)	750	300 spills/hr 1 sec. length	$4 \times 10^6 \bar{p}$ $+ 6 \times 10^6 \pi^-$ per $5 \times 10^{12} p$	$0.9 \times 10^{12} \bar{p}$ $1.2 \times 10^{12} \pi^-$
and				
b. 100 GeV positive secondary beam (charged configuration)	750	300 spills/hr 1 sec. length	$4 \times 10^6 p$ $+ 6 \times 10^6 \pi^+$ per $\sim 10^{10} p$	$0.9 \times 10^{12} p$ $1.4 \times 10^{12} \pi^+$
	1500			
II. 1000 GeV Accelerator 300 GeV Secondary Beam Transport (Doubler - current secondary transport)				
a. 300 GeV negative secondary beam (neutral configuration $\bar{\Lambda}^0 \to \bar{p}$)	750	100 spills/hr 10 sec. length	$1.5 \times 10^7 \bar{p}$ $+ 7.5 \times 10^7 \pi^-$ per $5 \times 10^{12} p$	$1.1 \times 10^{12} \bar{p}$ $5.6 \times 10^{12} \pi^-$
and				
b. 300 GeV positive secondary beam (charged configuration)	750	100 spills/hr 10 sec. length	$4 \times 10^7 p$ $+ 6 \times 10^7 \pi^+$ per $\sim 10^{10} p$	$3 \times 10^{12} p$ $4.5 \times 10^{12} \pi^+$
	1500			
III. 1000 GeV Accelerator 750 GeV Secondary Transport (Doubler - higher energy secondary beam)				
a. 750 GeV negative secondary beam (charged configuration)	750	100 spills/hr 10 sec. length	$1 \times 10^8 \pi^-$ per $10^{12} p$	$7.5 \times 10^{12} \pi^-$
and				
b. 750 GeV positive secondary beam (charged configuration)	750	100 spills/hr 10 sec. length	$1 \times 10^8 p$ per $10^{10} p$	$7.5 \times 10^{12} p$
	1500			

*A 300 GeV/c comparison of π^+/π^- is possible in this scenario with additional running time. However, with the advent of the Doubler in Scenario II the ability to get adequate luminosities of π^+ at 300 GeV/c is greatly enhanced. Therefore, we emphasize $\bar{p}/p$ in Scenario I.

III. Apparatus

The apparatus to be used in this experiment, which is shown in figure 1, is basically the E-537 large aperture spectrometer augmented by a fine grained liquid argon detector and a set of segmented Cerenkov counters for charged particle identification. The new devices are described in Appendices A and B of this proposal. The general parameters of the spectrometer are given in Table I below.

Table I

Vertical Aperture	±100 mrad
Horizontal Aperture	±200 mrad
$\int B.d\ell$	1089 kG inches

Resolutions (σ):	100 GeV	300 GeV	750 GeV
Mass ψ (3 GeV/c^2)	20 MeV/c^2	40 MeV/c^2	45 MeV/c^2
Mass Υ (10 GeV/c^2)	--	190 MeV/c^2	280 MeV/c^2
*Mass χ_ψ(3.5 GeV/c^2)	10 MeV/c^2	8 MeV/c^2	8 MeV/c^2
*Mass χ_Υ(10.0 GeV/c^2	--	11 MeV/c^2	11 MeV/c^2

**E resolution for γ	$\sigma \sim 6\% : \sqrt{E}$
P resolution for charged particles	$\sigma \sim 0.2\% . \sqrt{p^2 + 0.01p^4}$
Position resolution - Liquid Argon	$\sigma_x \sim 1$mm
Position resolution - Drift Chamber	$\sigma_x \sim 200$ microns
Mass π^o (from liquid Argon det.)	$\sigma/m \sim 4\%$ } 300 GeV/c
Mass η^o (from liquid Argon det.)	$\sigma/m \sim 3\%$ } 300 GeV/c
Resolving distance for two photons	$\sim$1cm

*Requires constraint of ψ(T) mass

**This resolution is due to the fine sampling which we have designed into our spectrometer. This resolution has already been achieved[23] with a liquid argon device with sampling similar to the device we intend to use.

IV. Physics Topic 1 - DIRECT PHOTONS

a. Event Rates

Direct photon production in proton-nucleon interactions has been observed by several experiments both at Fermilab[2] and CERN[3-5]. The currently existing data is shown as a function of $p_\perp$ in Figure 3. Attempts have been made by a number of theorists[6-10] to calculate the production of direct photons within the framework of QCD. These efforts have resulted in a consistent picture of direct photon production. In particular, the curves of Figure 3 represent the results of a calculation[6] which approximately fits all existing data. The sensitivity of the calculation to the choice of the intrinsic transverse momentum spectrum of the constituents is indicated by the $K_T = 0$ and 1 GeV/c dashed and solid curves.

Since no data exist at the present time for direct photon production by $\pi^\pm$ or $\bar{p}$ we have estimated the expected cross sections for these reactions from a QCD calculation similar to that which fits the proton-nucleon direct photon production. The Compton and annihilation processes have been calculated and summed using the usual formalism[24]:

$$\frac{d^2\sigma}{dp_\perp{}^2 dy} = \left[s\int_{X_{1_{min}}} \left(\frac{d\sigma}{dt'}\right)_C \left(\frac{1}{X_1 s+u}\right) \left(\sum e_q^2 \quad G.F + \quad \text{beam}\leftrightarrow\text{target}\right) \quad dX_1 \right.$$

$$\left. + s\int_{X_{1_{min}}} \left(\frac{d\sigma}{dt'}\right)_A \left(\frac{1}{X_1 s+u}\right) \quad \left(\sum e_q^2 \; F.F + \text{beam}\leftrightarrow\text{target}\right) \; dX_1 \right]$$

where: the $\frac{d\sigma}{dt'}$ are the appropriate subprocess cross sections for the Compton and annihilation diagrams, G and F are the gluon and quark structure functions with Q^2 dependence for the appropriate hadrons, s and u are the usual Mandelstam variables for the overall interaction, and t'

is the momentum transfer in the constituent subprocess. We have used the structure functions tabulated in references 25 and 26 with the gluon structure function modified to the strong glue form.[27] The intrinsic transverse momentum distribution of the gluons and partons is introduced via the Altarelli-Parisi method.[28,29] The average intrinsic transverse momentum is chosen to be 600 MeV/c to agree with that extracted from the μ pair production data of references 30, 31, and 32.

In figures 4a, b and 5a, b we show the direct photon cross sections which we expect for $p^{\pm}$ and $\pi^{\pm}$ interactions at 300 GeV/c as a function of $p_{\perp}$ and X_F in order to demonstrate several interesting features. It appears that at high $p_{\perp}$ the annihilation process is larger than the Compton process in the production of direct photons. This dominance of the annihilation process as shown in Figure 4a is true regardless of whether strong or weak glue structure functions are present. In addition, as shown in Figure 4a, b, the annihilation process is much larger in π^- and $\bar{p}$ induced reactions than in the π^+ or p interactions because of the presence of valence antiquarks of charge 2/3. These features lead to the expectation that the hadrons recoiling against the high $p_{\perp}$ direct photon will more often be the result of gluon fragmentation than quark fragmentation. In Figure 6 we show the integrated cross sections above $p_{\perp} = 3$ GeV/c as a function of beam energy in order to show the large increase in high $p_{\perp}$ cross section for direct photon production with increasing energy of the incident $\pi^{\pm}$ and $p^{\pm}$.

When an isoscalar target such as deuterium is employed, the difference of the $\bar{p}$ and p or the π^- and π^+ induced direct photon signals should be the contribution due to the annihilation process and should contain indications of gluon jets. In addition the difference between the π^+ and π^- cross sections should be free of residual backgrounds to

the direct photon production which are due to photons from π^0 and η decay since π^0 and η production should be the same for π^+ and π^- interactions with D_2 by isospin argument. The same background statement should be approximately true for $\bar{p}/p$ differences, although in this case an isospin argument cannot be made. In addition the $pD \rightarrow \gamma X$ and, to a lesser extent, the $\pi^+D \rightarrow \gamma X$ reactions are dominated by the Compton process. Therefore, by examining these reactions it is possible to study an almost pure Compton process and to search for evidence of quark jets. However, in this case the direct photon backgrounds must be estimated from the observed π^0 and η production and taken into account.

Using the above QCD calculation, direct photon event rates for each of the three beam scenarios have been calculated and are given in Figures 7-12 as a function of $p_\perp$ and X_F. The large numbers of direct photons which are produced in each scenario are adequate to probe the kinematic boundaries in both X_F and $p_\perp$. Unlike the production of dileptons (which is suppressed by a factor of α relative to direct photons at a given X_F and $p_\perp$), the problem with direct photons is not one of event rate, but rather one of backgrounds. Both by the technique of taking differences of cross sections and by eliminating π^0 and η photons to minimize these backgrounds we will achieve clean direct photon signals.

b. <u>Backgrounds to direct photons</u>

The major backgrounds for the direct photon part of the experiment arise from several sources:

1. Single photons from π^0, η (ω^0, η', χ, etc.) decay in which the other photon is lost outside the liquid Argon electromagnetic detector or in the beam hole.
2. Asymmetric π^0, η decay in which one of the photons from the π^0 or η is so low in energy that it is not recognizable in the neutral detector.
3. Events in which one photon from a π^0 decay converts in the

deuterium target or in another part of the spectrometer and the e^+e^- pair is not recognized as such in the spectrometer.

4. Coalescing photons from π^0 decay.

5. Neutral hadrons.

We have estimated backgrounds 1-4 by using measured π^0 and η fluxes.[33 - 35] For the case of $\bar{p}p \to \pi^0 X$ we have assumed that the cross section is approximately the same as that of $pp \to \pi^0 X$. We use the scaling form

$$E\frac{d^3\sigma}{dp^3} = A\, p_\perp^{-N}(1-X_R)^M \qquad X_R = \sqrt{X_\perp^{\,2} + X_F^{\,2}}$$

with N=9, M=5, and $A = 3.8 \times 10^{-27} cm^2/GeV^2$/nucleon. This form fits the data of reference 33 for pN interactions. The $\pi^\pm p \to \pi^0 X$ cross sections are taken from reference 34:

$$E\frac{d^3\sigma}{dp^3} = A'\ (1 - X_D)^F/(p_\perp^{\,2} + 0.97)^N \qquad X_D = \sqrt{X_\perp^{\,2} + (X_F - 0.14)^2}$$

with N=5, F=3, and A' $1.1 \times 10^{-26} cm^2/GeV^2$/nucleon. An η/π^0 ratio of 0.5 measured in these two experiments[33,34] is used in simulating the background due to η. The production of ω^0, η', χ has been measured[35] and the backgrounds they cause are insignificant. Using these cross sections we have simulated in a monte carlo the π^0 and η flux and investigated the properties of our spectrometer.

In order to eliminate background photons from η or π^0 decay in our data sample we compute the invariant mass of all two photon combinations. All residual unpaired photons are direct photon candidates and form a major background. Clearly, the energy and position resolution of the detector are important in providing positive identification of a two-photon pair as a π^0 or an η. The properties of the detector described in Appendix A are such that the mass resolutions at 300 GeV/c are $\sigma_{\pi^0} \sim 6 MeV/c^2$ and $\sigma_\eta \sim 16 MeV/c^2$. This makes the effect of mispairing negligible.

The relative importance of the various backgrounds 1-4 varies with the energy of the beam which is available. At the lower energies the dominant background is due to photons lost outside the acceptance of the neutral detector. As the energy increases the loss of photons in the 5" x 5" beam hole of the neutral detector becomes more serious but never exceeds the loss of photons outside the fiducial region of the detector. In order to minimize the unpaired photons which have their mate lost outside the aperture a 10" region around the outer edge of the neutral detector has been excluded from the acceptance for direct photon detection. Any photon in this 10" border is tried in combination with every photon to see if a π^0 or an η is formed, but no unpaired photon in this region is accepted in the direct photon data sample.

The second most serious background is the loss of low energy photons which are not recognizable in the detector. We have taken a lower limit of 300 MeV for the energy cutoff. Further experience with the liquid argon device may allow us to lower that limit.

The third background which we have considered comes from events in which a photon converts either in the deuterium target or in a wire chamber or Cerenkov mirror in the spectrometer and in which the e^+e^- do not both make it into the neutral detector. We have assumed here that both the e^+ and e^- must be in the acceptance of the neutral detector in order for the event to be recognized as a conversion. In practice a less restrictive requirement than this may effectively eliminate this background. Finally, due to the granularity (1 cm strips) and two-dimensional nature of our neutral detector, the coalescing of photons from π^0 decay is no problem in any of the scenarios and makes a negligible contribution to the backgrounds.

Neutral hadrons which shower early in the liquid argon detector are the final background to which the direct photon measurement is vulnerable. In order to estimate this we take as a worst case the experience of the ISR experiments of Ref. 3. By examining the longitudinal and transverse development of showers in their liquid argon detector they were able to eliminate most of the neutral hadron background. From their experience we estimate that this background can be reduced by a factor of 10. The residual neutral hadron background should then be less than 1% of the real direct photon signal.

In Figs. 7-12 we show our estimates of the residual background of single photons which have not been paired into an η or π^0 vs. $p_\perp$ and X_F. Both at high $p_\perp$ and X_F the signal to background improves. For the high $p_\perp$ and X_F regions where the signal/background ratio is large, the direct photon flux will provide a clean signal for extraction of structure functions.

c. Direct Photon Trigger and Trigger Rate

In order to trigger on direct photon events, the liquid argon shower detector will be divided into 60 regions in the X (i.e., horizontal) dimension which we will refer to as roads. Each road will be associated with a number of elements of the CPX hodoscope (charged particle hodoscope-X dimension, see Figure 1). These roads will overlap in order to accommodate the tails of electromagnetic showers. A photon in a particular road will have the signature of:

1. No CPX elements firing in that road (neutral requirement);
2. E_{road} > energy threshold. This energy threshold must be a function of the X location of the specific road and is equivalent to a crude $p_\perp$ cut.

3. The energy from the first 12 radiation lengths of the liquid argon detector > 2/3 E_{road} (neutral hadron rejection by longitudinal shower cuts).

We have estimated the photon trigger rates which arise mainly from real photons from π^0 or η decay which have sufficient energy to survive the crude $p_\perp$ cut. The results for each beam energy are given below:

Scenario I	100 GeV $p^\pm/\pi^\pm$	90 triggers/second	($p_\perp$ cut $\leq$ 2.5 GeV/c)
Scenario II	300 GeV $p^\pm/\pi^\pm$	50 triggers/second	($p_\perp$ cut $\leq$ 3.0 GeV/c)
Scenario III	750 GeV $p/\pi^\pm$	75 triggers/second	($p_\perp$ cut $\leq$ 3.0 GeV/c)

The total trigger rate including real direct photon and fake single photons is therefore not expected to exceed 100 per second in any scenario. Furthermore, the rate can be sensitively controlled by minor adjustments of the $p_\perp$ trigger.

V. Physics Topic 2 - RESONANCE STUDY

a. Event Rates/Backgrounds

At the same time in which we are accumulating data to measure the direct photon cross sections produced by $p^{\pm}$ and $\pi^{\pm}$ beams, we plan to continue to use our di-muon trigger to accumulate a large sample of resonance decays (such as χ or B) which result in a ψ in the final state. In addition, if the highest energy negative beam (750 GeV/c π^-) is used, the yield of Υ's should be adequate to study the upsilonium system. Figure 13 shows the expected large ratio of π^- p production of upsilons and the increase of the cross section with $\sqrt{s}$. The combination of these factors makes the detection of hadroproduction of upsilonium states with the 750 GeV π^- beam possible. Table II shows either the expected number of events of the various heavy quark states, which we will collect in a given 1500 hour scenario, or the sensitivity which can be achieved for the states which have yet to be observed. The Υ and B numbers at 750 GeV/c are quoted only for the π^- beam.

Table II

Resonance Production

Scenario →	100 GeV $\bar{p}/p$	100 GeV π^-/π^+	300 GeV $\bar{p}/p$	300 GeV π^-/π^+	750 GeV π^-
$\psi \to \ell^+\ell^-$	11K/6.5K	31K/33K	72K/130K	450K/360K	490K
$\psi' \to \ell^+\ell^-$	.2K/.1K	.6K/.7K	1.5K/2.8K	9K/7K	10K
$\chi(3.51) \to \gamma\psi \to \gamma\ell^+\ell^-$, $\chi(3.54) \to \gamma\psi \to \gamma\ell^+\ell^-$, $\chi(3.42) \to \gamma\psi \to \gamma\ell^+\ell^-$, $2'p_1 \to \gamma\psi \to \gamma\ell^+\ell^-$	** 2.5K/1.5K	7K/8K	17K/31K	105K/84K	123K
$\Upsilon(9.45) \to \ell^+\ell^-$	--	--	30/55	160/125	950
$\Upsilon(10.00) \to \ell^+\ell^-$	--	--	10/18	50/40	300
$\Upsilon(10.32) \to \ell^+\ell^-$	--	--	2/4	10/8	50
χ_Υ family *	--	--	10/20	58/45	340
$B(5.3) \to \chi K \to \gamma\ell^+\ell^- K$, $B(5.3) \to \chi K\pi \to \gamma\ell^+\ell^- K\pi$ ***	1/1	.3/.3	.3/.1	.05/.06	.07

* Hadroproduction not yet observed. Ratio of χ_Υ/Υ production assumed to be the same as χ_ψ/ψ.

** The relative cross sections for the various χ states are unknown. We have used the average value of the ratio of all $\chi \to \gamma\psi$ hadroproduction taken from recent measurements of $.36 \pm .05$.

*** Not yet observed. Sensitivity for $B \cdot \sigma$ are quoted in pbarn/event.

The cross sections for $\pi^{\pm}$ and $p^{\pm}$ production of ψ, ψ' and the π^- production of Υ have been taken from reference [36-38]. The production cross sections for $\pi^- N \to \Upsilon X$ has been extrapolated to higher energy assuming that the pN and $\pi^- N$ cross sections (as shown in figure 13) become equal at infinite energies. The ratio of the production of the various upsilonium states in π^- interactions is taken to be the same as the ratios observed in pN interactions[39]. Finally, while the ratio of the $\pi^-/\bar{p}$ cross sections is obviously a function of energy for experiments done in this energy regime we have taken $\pi^- N$ equal to $\bar{p}N$ for resonance production at all energies.

Using these data and assumptions we can estimate the level of χ production from the various measurements[11-15] of the ratio of χ hadroproduction to ψ hadroproduction. We have taken the observations of reference [13] for $\pi^- N \to \chi X$ at 175 GeV/c as most current and appropriate to our experiment. Using their result of .36±.05 for $\frac{\pi^- N \to \chi X}{\pi^- N \to \psi X}$ we have estimated the total χ production given in Table II. However, the χ production and the relative contributions of the various χ states are unknown. With the good photon and charge particle resolution of our spectrometer and its ability to lower the combinatorial background by rejecting π^0 or η photons, we should be able to resolve the various χ states. As an indication of the performance of the spectrometer we show in Figure 14A the expected $\gamma\psi$ mass spectrum for $\bar{p}p$ interactions at 100 GeV/c. (In Figure 14B the comparable plot for $\pi^- p$ interaction which will be accumulated simultaneously is shown.) We have assumed for the purpose of preparing Figure 14 that all the 2^3P_J states were produced with equal probability (in contradiction to the prediction of the gluon fusion model[16]) and we have constrained the ψ mass to 3.1 GeV/c^2. The 2^1p_1 state was ignored since it has not been observed in e^+e^- reactions. However there is a possibility of observing this state directly produced in hadronic reactions

since its production in e^+e^- via the chain $e^+e^- \to \psi \to \gamma\chi \to \gamma\gamma\psi$ may be suppressed because of a small $\psi' \to \gamma\chi$ branching ratio. The branching ratios for $\chi \to \gamma\psi$ have been taken from reference 40. The combinatorial background has been estimated by superimposing ψ events on the background of π^0 and η photons which have been estimated from $\bar{p}p$ bubble chamber events[41]. All reconstructed π^0's and η's have been eliminated from the photon sample. It is clear that the expected photon energy resolution of $\sigma \sim 6\% \cdot \sqrt{E}$ is good enough to achieve clean separation of the χ states. We have investigated the resolution requirement and expect that good separation of the states at 100 GeV/c can be achieved even if the photon energy resolution decreases to $8\% \cdot \sqrt{E}$. When the beam energy is increased to 300 or 750 GeV/c, the decrease in charged particle momentum resolution is balanced by the increase in photon energy resolution such that the χ resolution remains relatively constant. We therefore expect to be able to resolve χ_ψ and χ_Υ states with 10/1 relative strengths at all energies.

We plan at the higher energies (300, 750 GeV/c) to search for hadronic production of χ_Υ. Since nothing is known at this time about χ_Υ hadroproduction, we have assumed that the ratio of hadroproduction of χ_Υ to hadroproduction of the Υ is the same as that of the charmonium states in order to obtain the numbers in Table II. After detection of these states an attempt will be made to measure their relative cross sections for comparison with gluon fusion models.

Finally we intend to search our data samples for evidence of the expected [19] beauty decays into $\psi K\pi$ or ψK and for the first time to search for $\chi K\pi$ or χK. The experimenters of reference 42 have placed upper limits on the ψK^0 and $\psi K^0\pi^\pm$ modes of 0.08 and 0.51 nb/nucleon respectively from a data sample of 40K ψ events. These limits correspond to a sensitivity of 11pb/event, to be compared with the sensitivity of the proposed experiment. In addition, at the higher energies not only will our

luminosity be greater than the previous searches, but we should gain large factors in cross section because our center of mass energy is higher and beauty production is expected to increase rapidly with energy near threshold.

B. Trigger Rate for Di-Muon Resonance Studies

The trigger with which we plan to accumulate our resonance data is the di-muon trigger of E-537 Phase I. We expect to use the same trigger processor[42] to impose a di-muon mass cut to further eliminate spurious triggers. Without the copper absorber of our Phase I experiment the major contribution to the trigger rate will be two decaying pions producing a di-muon trigger. We have estimated from bubble chamber data the trigger rates which are given below for the expected interaction rate at each beam energy.

Beam Energy	All Di Muon Triggers per sec	Di Muon Triggers/sec After 2 GeV Trigger Processor Cut
100 GeV	2600	∿125
300 GeV	2900	∿125
750 GeV	1700	∿125

As can be observed the rate which the trigger processor is required to handle is quite reasonable and the number which pass the trigger processor cut can be handled by the online data acquisition system.

REFERENCES

1. E-537 Proposal, Nov. 1977, Jan. 1978/Approval letter from E. Goldwasser April 1978.

2. R. M. Baltrusaitis et al., Physics Lett. 88B, (1979) 372.

3. M. Diakonou et al., Physics Lett. 87B, (1979) 292.

4. E. Amaldi et al., Physics Lett. 84B (1978) 240.

5. A. Angelis et al., Physics Lett. 94B (1980) 106.

6. L. Cormell and J. F. Owens, contributed paper, XXth International Conference, Madison, Wisconsin (1980).

7. A. P. Contogouris, S. Papdapoulos, and C. Papavassiliou, Preprint McGill University invited paper XXth International Conference, Madison, Wisconsin (1980).

8. F. Halzen and D. Scott, invited paper, XXth International Conference, Madison, Wisconsin (1980)., University of Wisconsin preprint DOE-ER/00881-15.

9. K. Kata and H. Yamamoto, preprint, University of Tokyo, UT-335 Jan. (1980).

10. R. Ruckl, S. J. Brodsky, J. F. Gunion, Physical Rev., D18 (1978) 2469.

11. T. B. W Kirk et al., Phy. Rev. Lett. 42 (1979) 619.

12. Y. Lemoigne, Proceedings of the 1979 International Symposium on Lepton and Photon Interactions at High Energies (1979) 524.

13. Y. Lemoigne et al. XX International Conference on High Energy Physics, Madison, Wisconsin (1980).

14. J. H. Cobb et al., Physics Lett., 72B (1978) 497.

15. A. G. Clark et al., Nuclear Physics, B142 (1978) 29.

16. C. E. Carlson and R. Suaya, Phys. Rev. D14 (1976) 3115, D15 (1977) 1416, D18, (1978) 760.

17. B. L. Ioffe, Phy. Rev. Lett., 39 (1977) 1589.

18. R. Barate et al, XX International Conference on High Energy Physics, Madison, Wisconsin (1980).

19. H. Fritzsch, Workshop on New Flavors, College de France (1979), Physics Letters, 86B (1979) 343.

20. Negative beam yields have been measured by the E-537 experiments at 400 GeV/c and are approximately as expected for the $\bar{\Lambda}^{o}$ and charged beams. The 1000 GeV/c yields are predicted from these measurements. The expected positive yields are estimated from the ratio of positive to negative particle yields extracted from W. F. Baker et al., Fermilab-78/79-Exp 71100.104, (1978) and W. F. Baker et al., M1 Beam Design Report.

21. B. Cox, Fermilab Report 79/1, 0090.01, January (1979)

22. B. Cox et al., P-West High Intensity Secondary Beam Area Design Report March (1977).

23. C. Cerri and F. Sergrampietri, Nuclear Instruments and Methods, 141 (1977) 207.

24. F. Halzen and D. Scott, Physical Rev., D18 (1978) 3778.

25. J. F. Owens and E. Reya, Phys. Rev., D17 (1978) 3003.

26. R. P. Feynman, R. D. Field, G. C. Fox, Phys. Rev., D18 (1978) 3320.

27. J. F. Owens, A. P. Contagouris, private communication.

28. G. Altarelli, G. Parisi, R. Petronzio, Phys. Lett., 76B (1978) 356.

29. See for example R. D. Field, Cal Tech Preprint CALT-68-739 for a discussion of the application of the Altarelli-Parisi method.

30. D. C. Hom et al, Phys. Rev. Lett. 36 (1976) 1239, and 37 (1976) 1374.

31. S. Witterb et al., Phys. Rev. Lett 39 (1977) 252.

32. W. R. Innes et al., Phys. Rev. Lett. 39 (1977) 1240.

33. R. M. Baltrusaitis et al., Phys. Rev. Lett., 44 (1980) 122.

34. G. Donaldson et al., Phys. Rev. Lett. 40 (1978) 684.

35. C. Kourkoumelis et al., Phys. Lett, 84B (1979) 271, ibid 84B (1979) 277 M. Diakonou et al., Phys. Lett. 89B, (1980), C. Kourkoumelis et al., Phys. Letters 81B (1979) 405.

36. D. DeCamp et al., E.P.S. Meeting Proceedings, CERN (1979).

37. J. Badier et al., CERN/EP 79-61 (1979).

38. J. Badier et al., CERN/EP 80-149 (1980).

39. W. R. Innes et al., Phys. Rev. Lett., 39 (1977) 1240.

40. Particle Data Group, Reviews of Modern Physics, Vol. 52, (1980).

41. We have used the 100 GeV/c $\bar{p}p$ data of Fermilab experiment E311 for this simulation of backgrounds.

42. T. Kostarakis et al., Topical Conference on the Application of Microprocessors to High Energy Physics Experiments, CERN, 4 May 81.

43. T. Droege et al., IEEE Transactions on Nuclear Science, NS-25, 1 (1978) 687.

44. H. Burkhardt et al., Preprint DESY 80/10 (1980).

45. K.J. Anderson et al., Phys. Rev. Lett., 42 (1979) 944, K. J. Anderson et al., XVIII Conference in High Energy Physics, Tbilisi, U.S.S.R. (1976)

E-537 PHASE II
SPECTROMETER

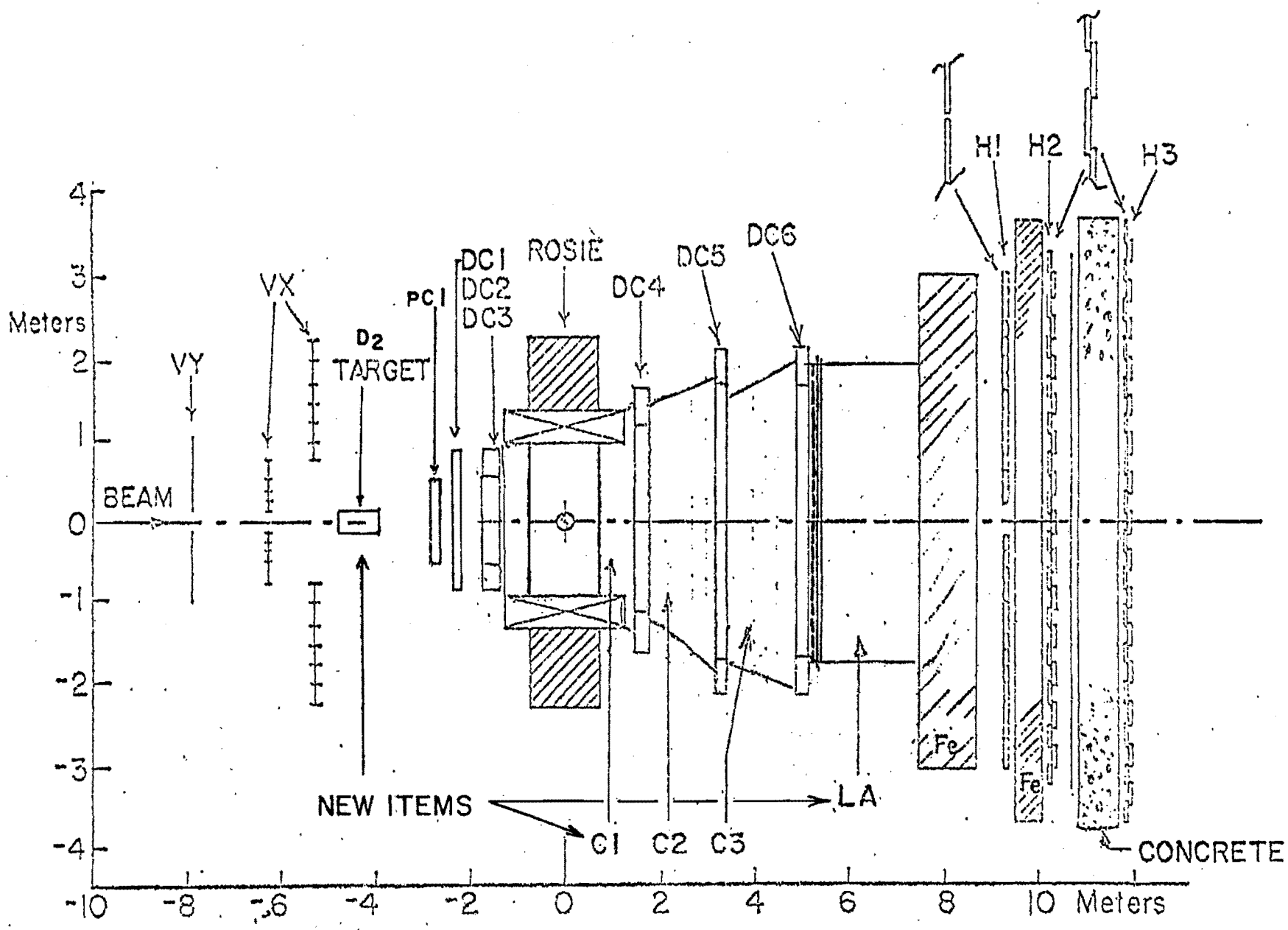

FIGURE 1

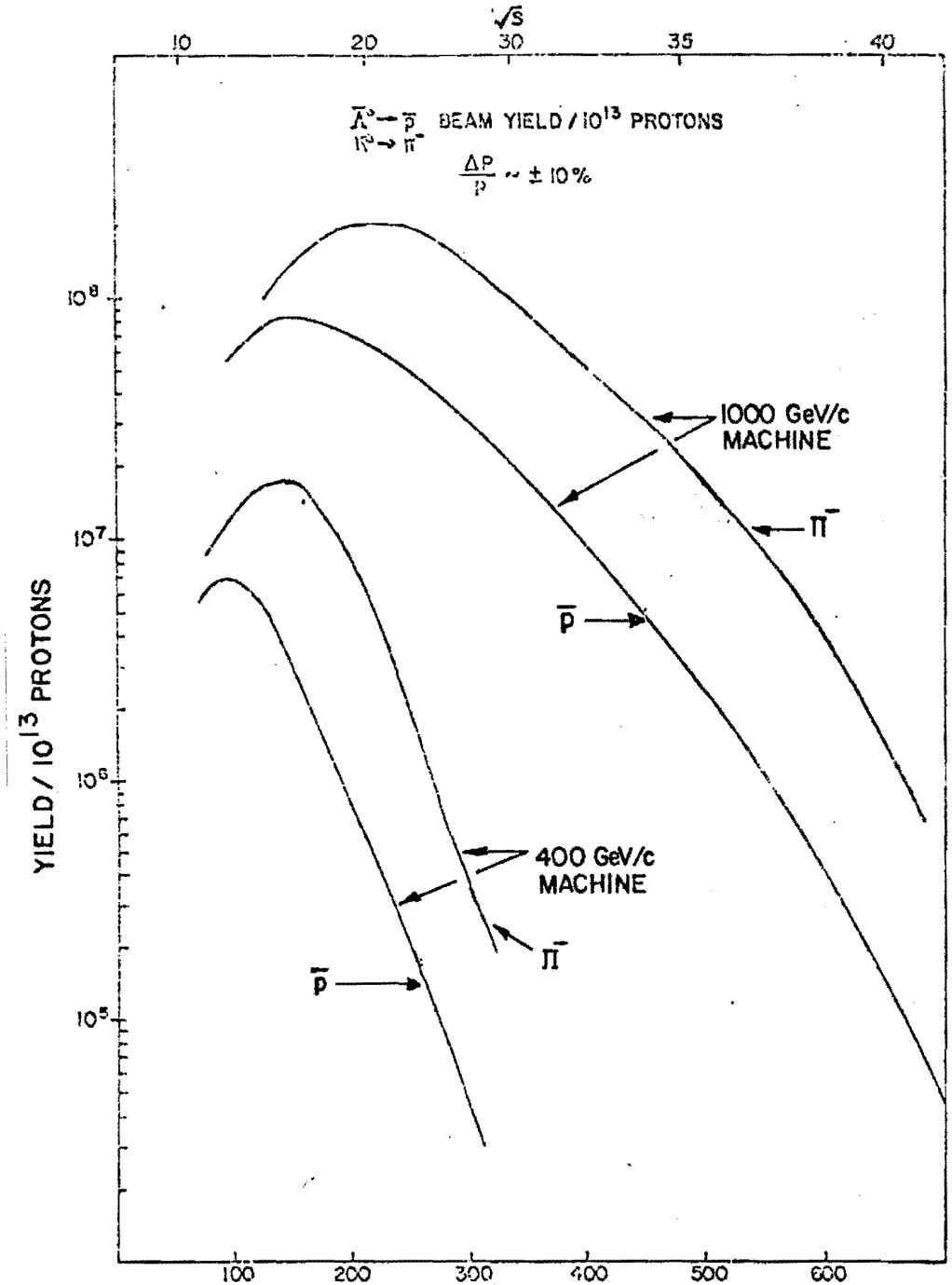

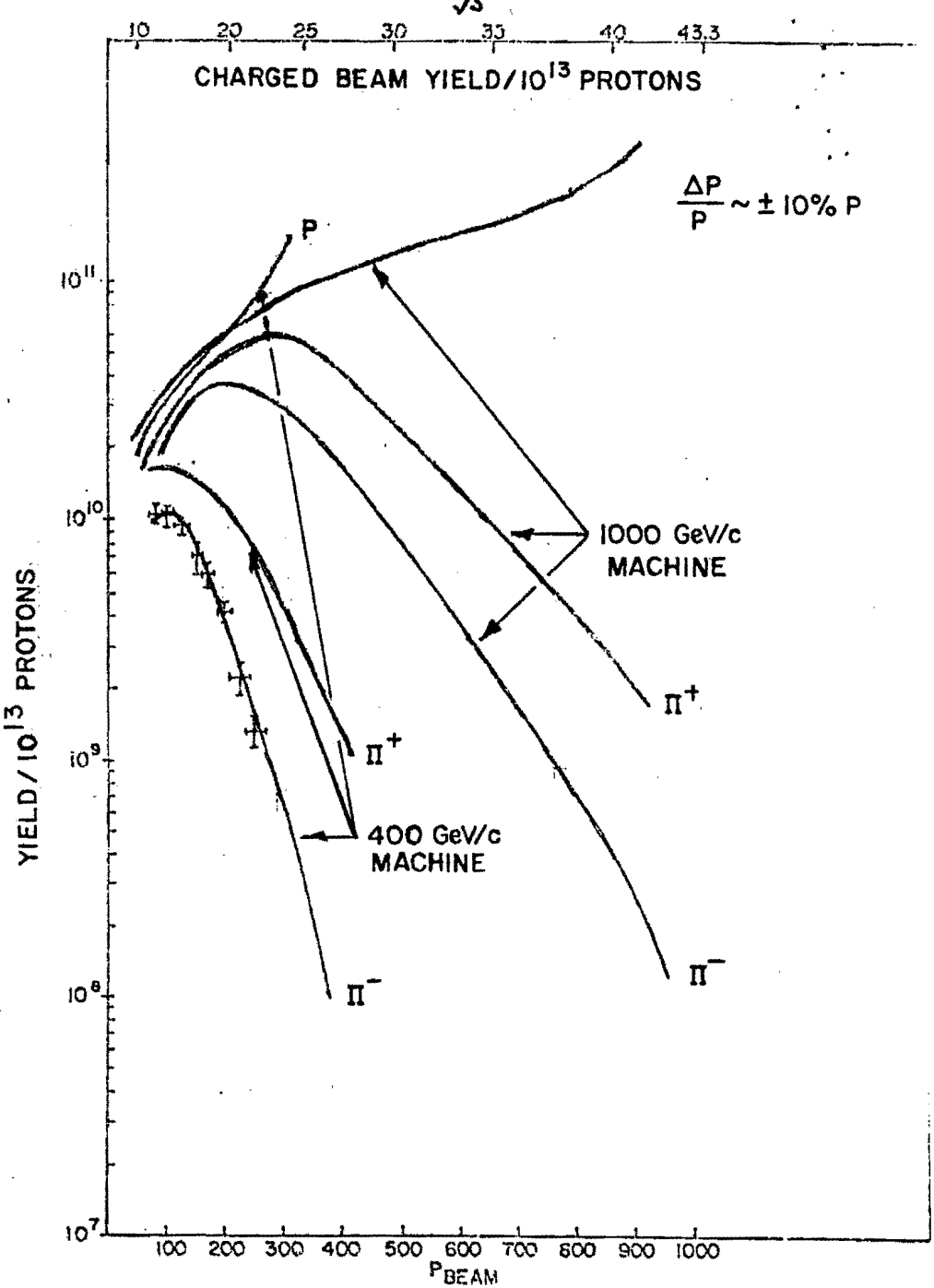

FIGURE 2
HIGH INTENSITY LABORATORY
YIELD CURVES

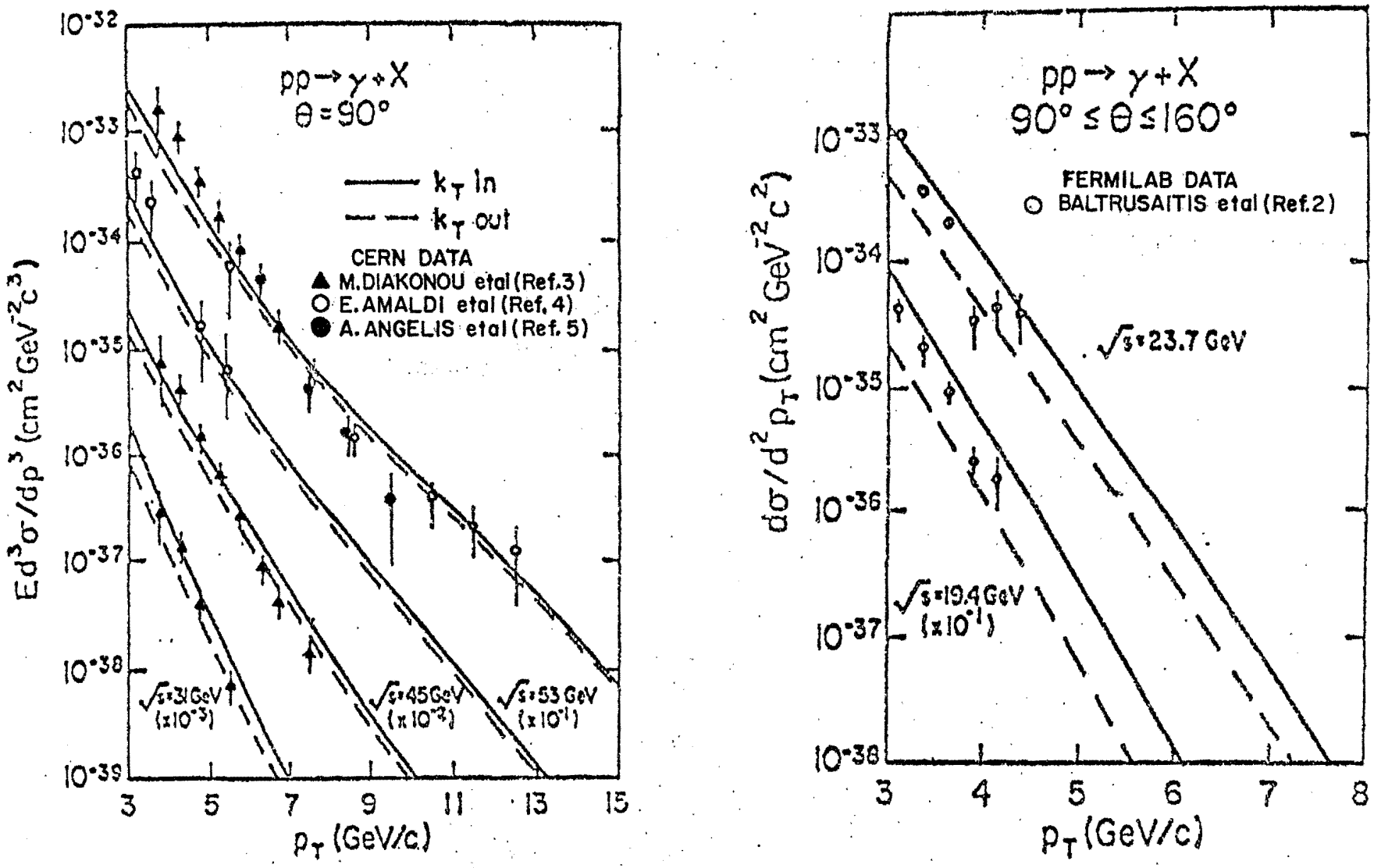

FIGURE 3

EXISTING pp → γX DATA

FIGURE 4a

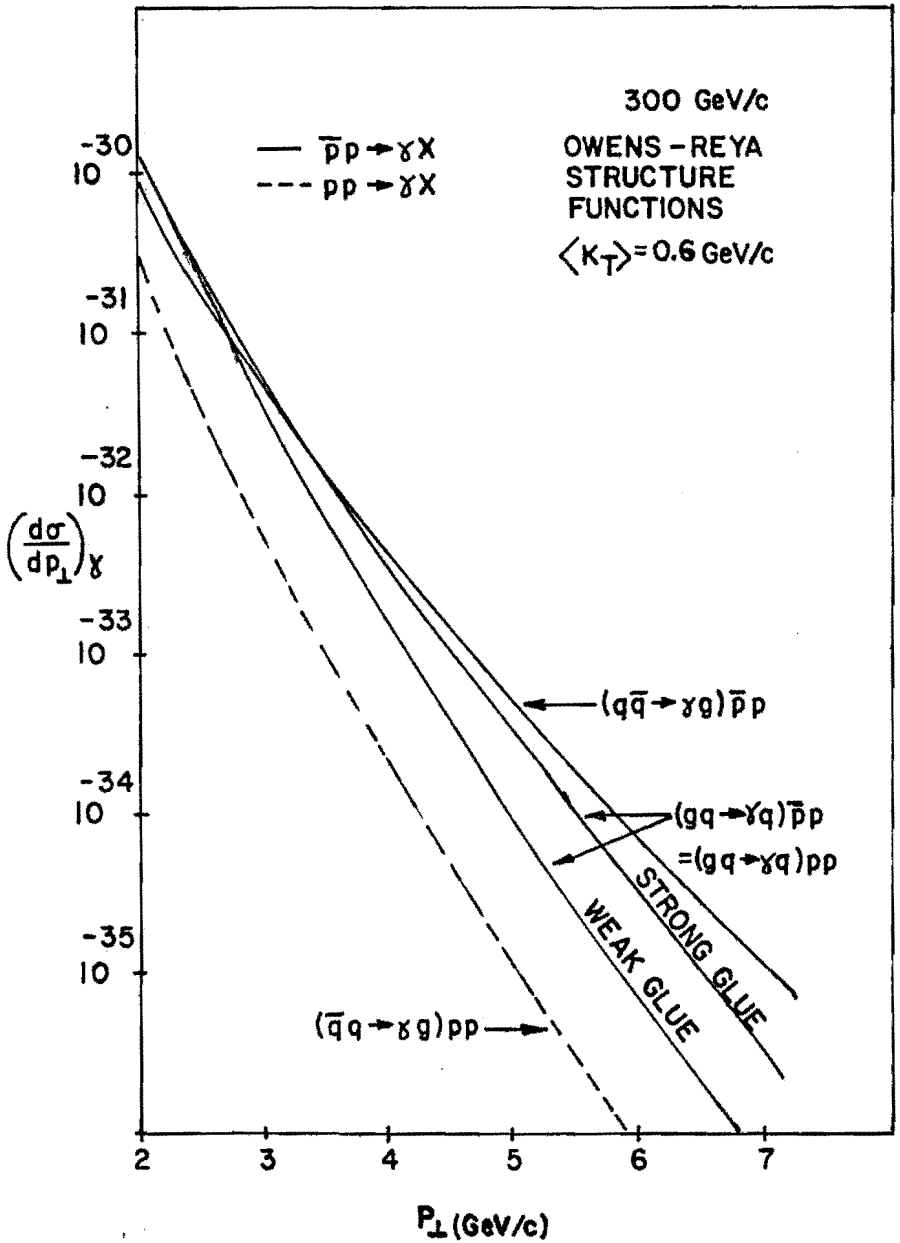

FIGURE 4b

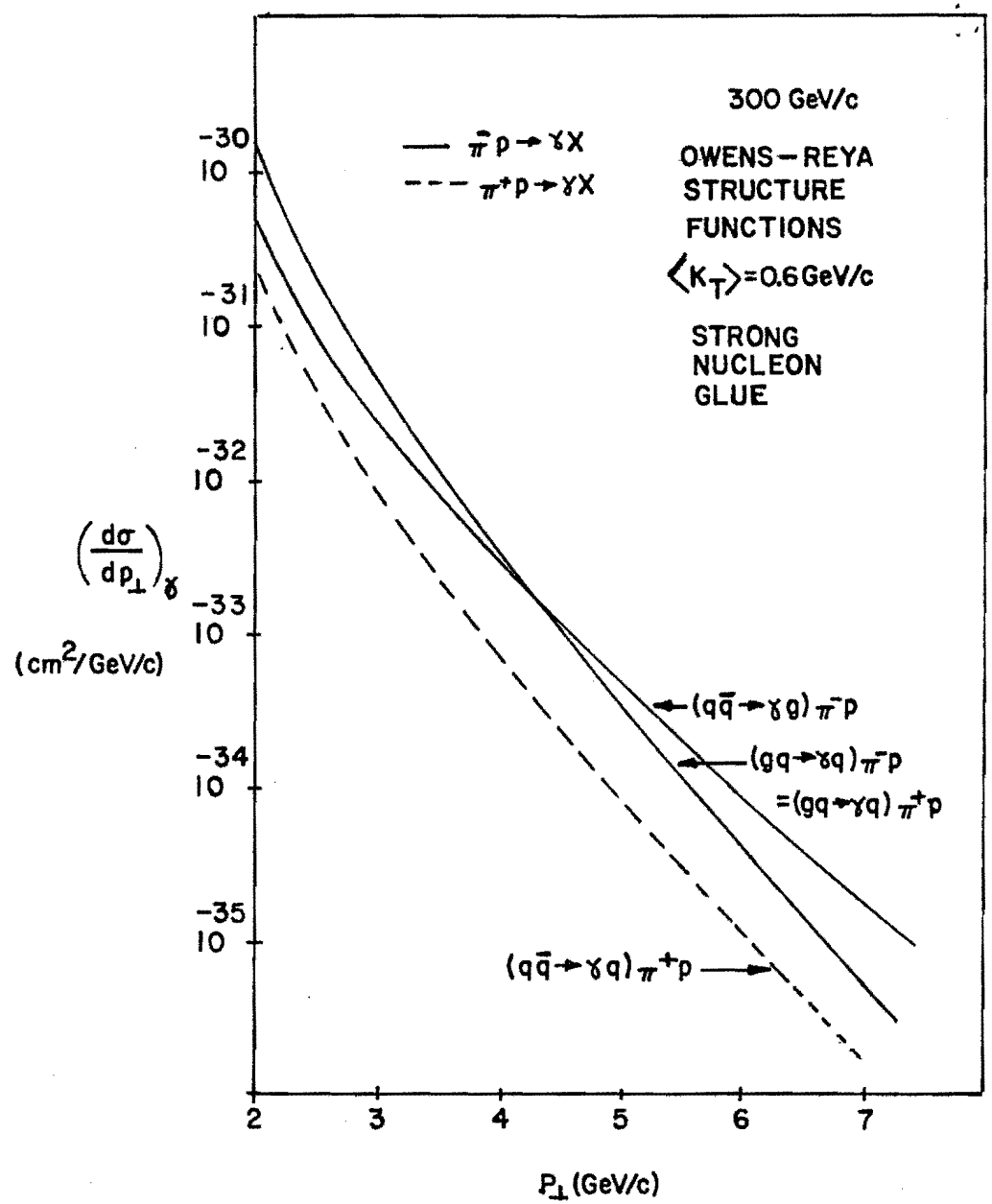

CROSS SECTIONS Vs $P_\perp$
FOR DIRECT PHOTON
PROCESS

FIGURE 5a

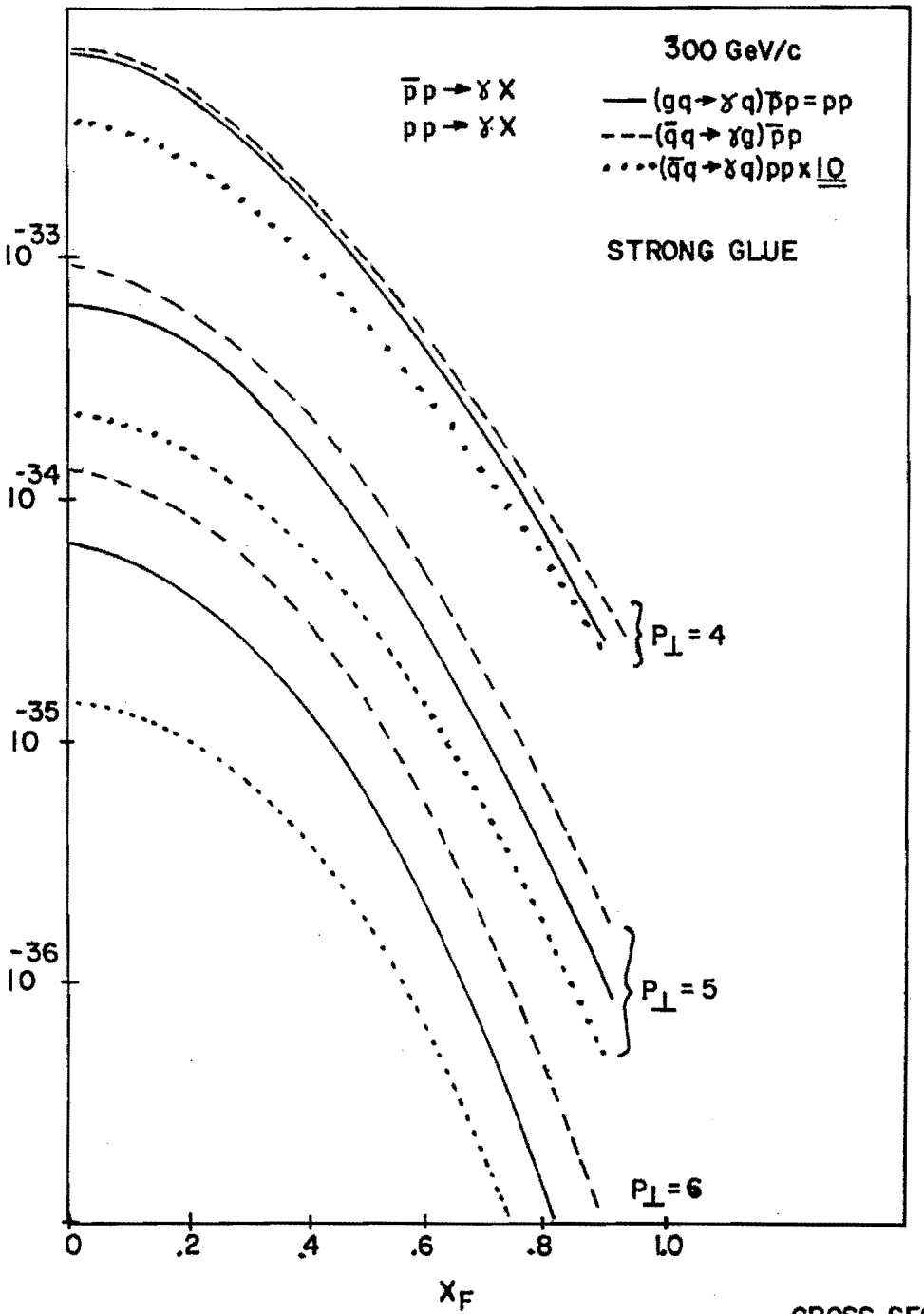

FIGURE 5b

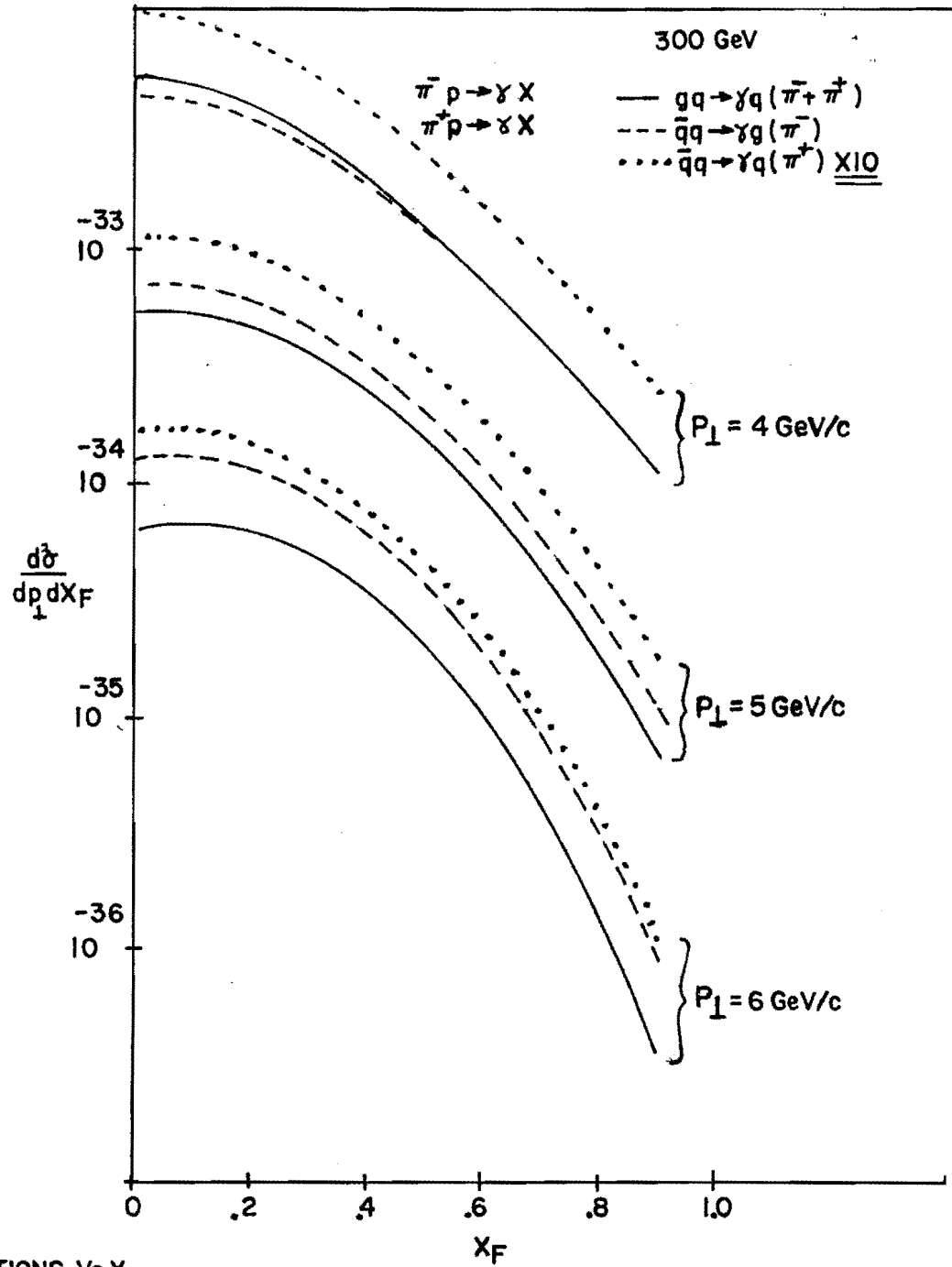

CROSS SECTIONS Vs X_F
FOR THE DIRECT PHOTON
PROCESS

FIGURE 6

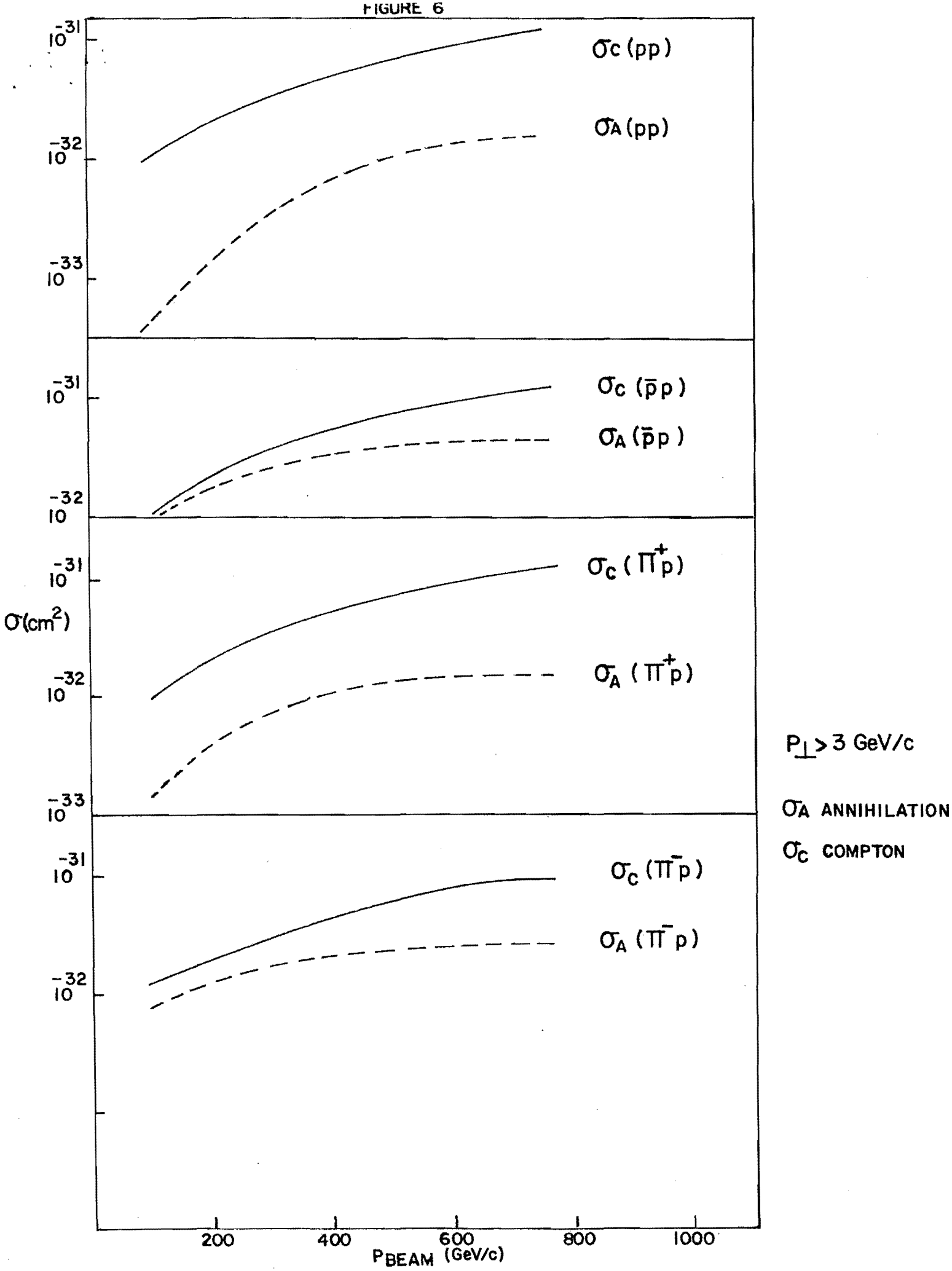
10^{-31}
10^{-32}
10^{-33}
σ_C (pp)
σ_A (pp)
σ_C ($\bar{p}$p)
σ_A ($\bar{p}$p)
σ_C (π^+p)
σ_A (π^+p)
σ_C (π^-p)
σ_A (π^-p)
σ(cm^2)
200
400
600
800
1000
P_{BEAM} (GeV/c)
$P_\perp > 3$ GeV/c
σ_A ANNIHILATION
σ_C COMPTON

FIGURE 7a

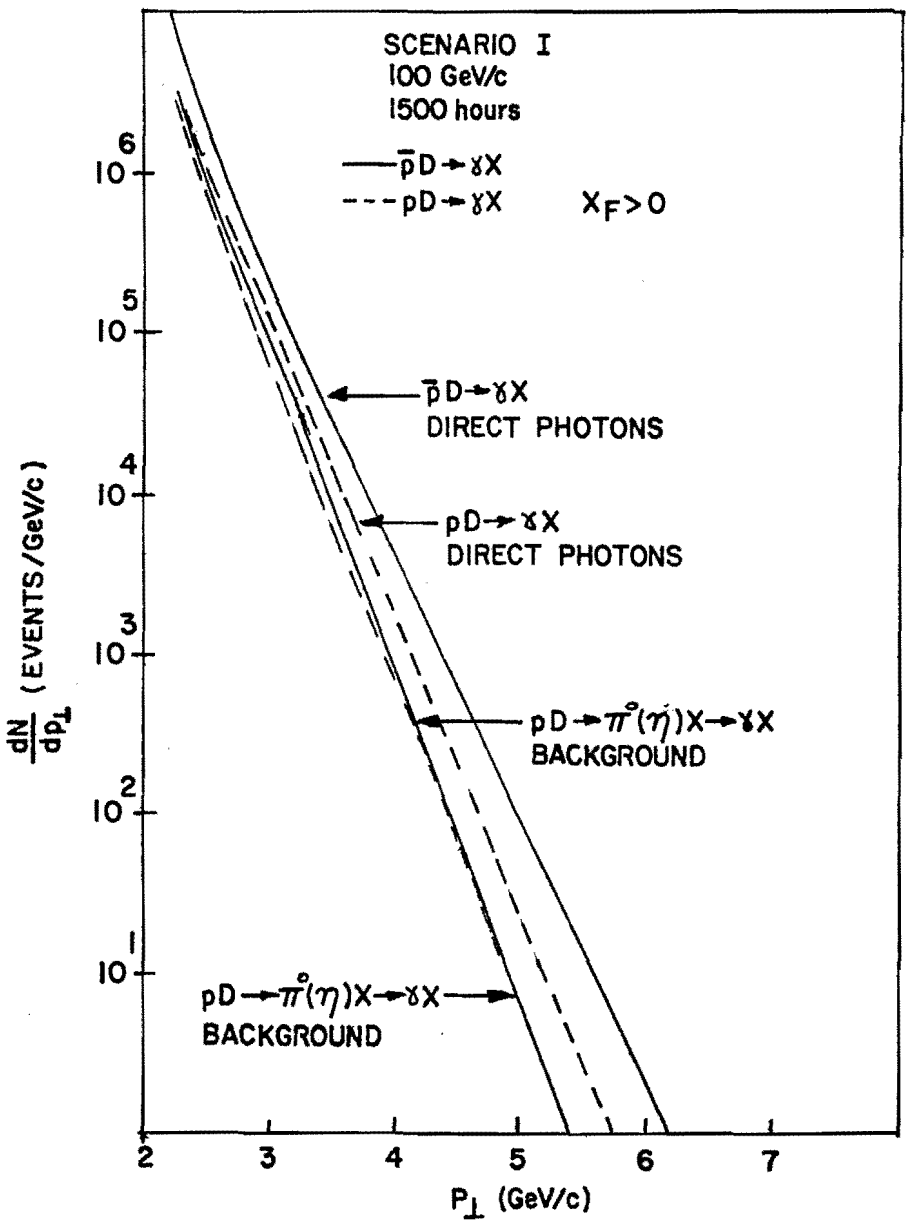

FIGURE 7b

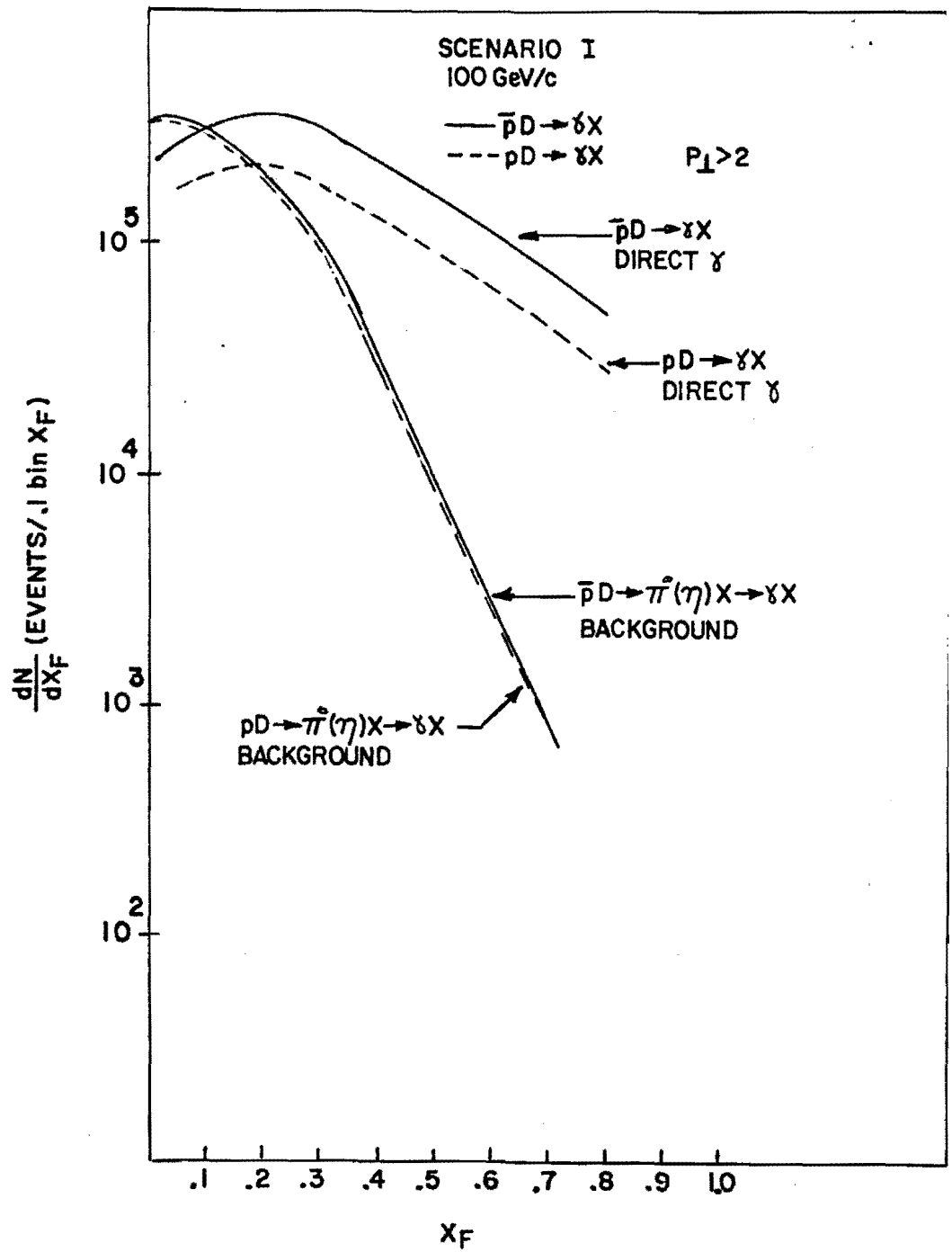

FIGURE 8a

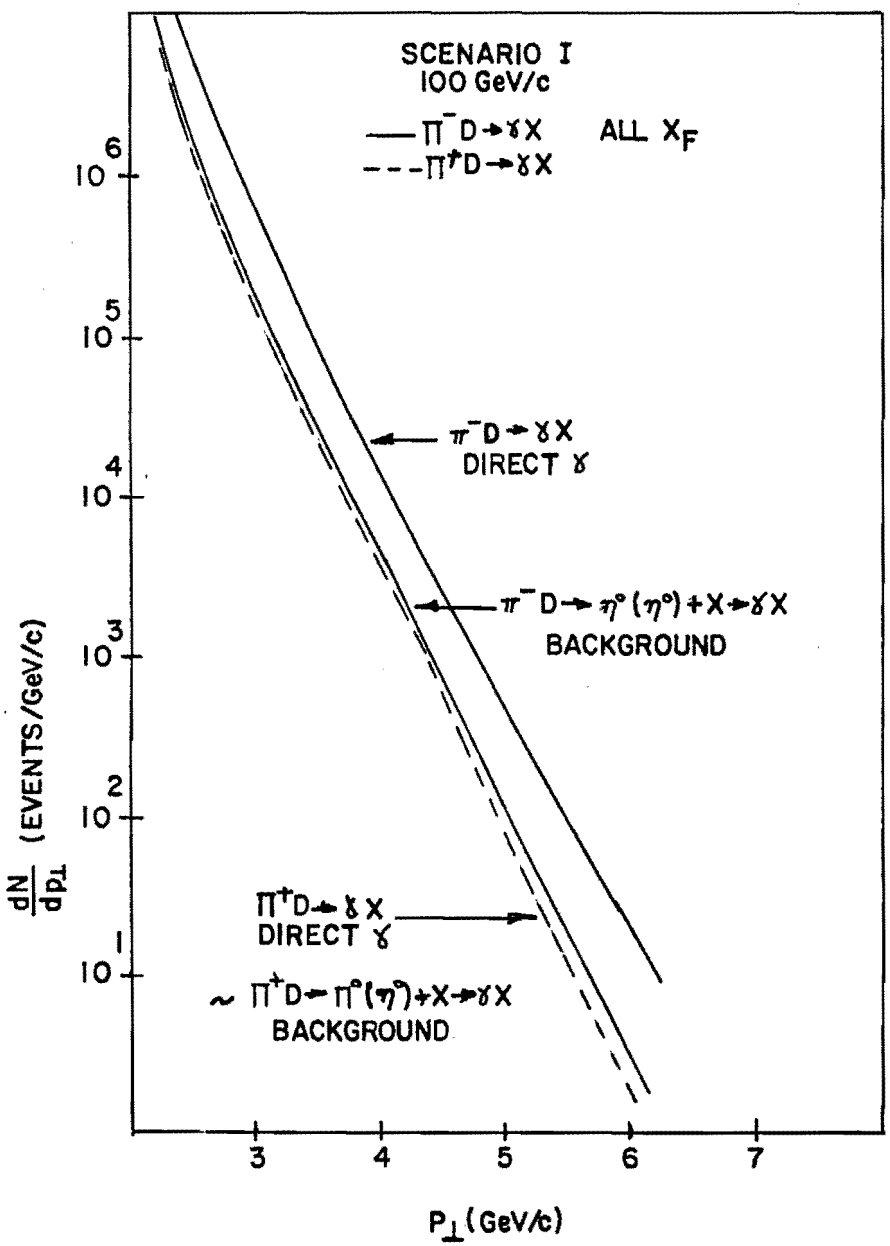

FIGURE 8b

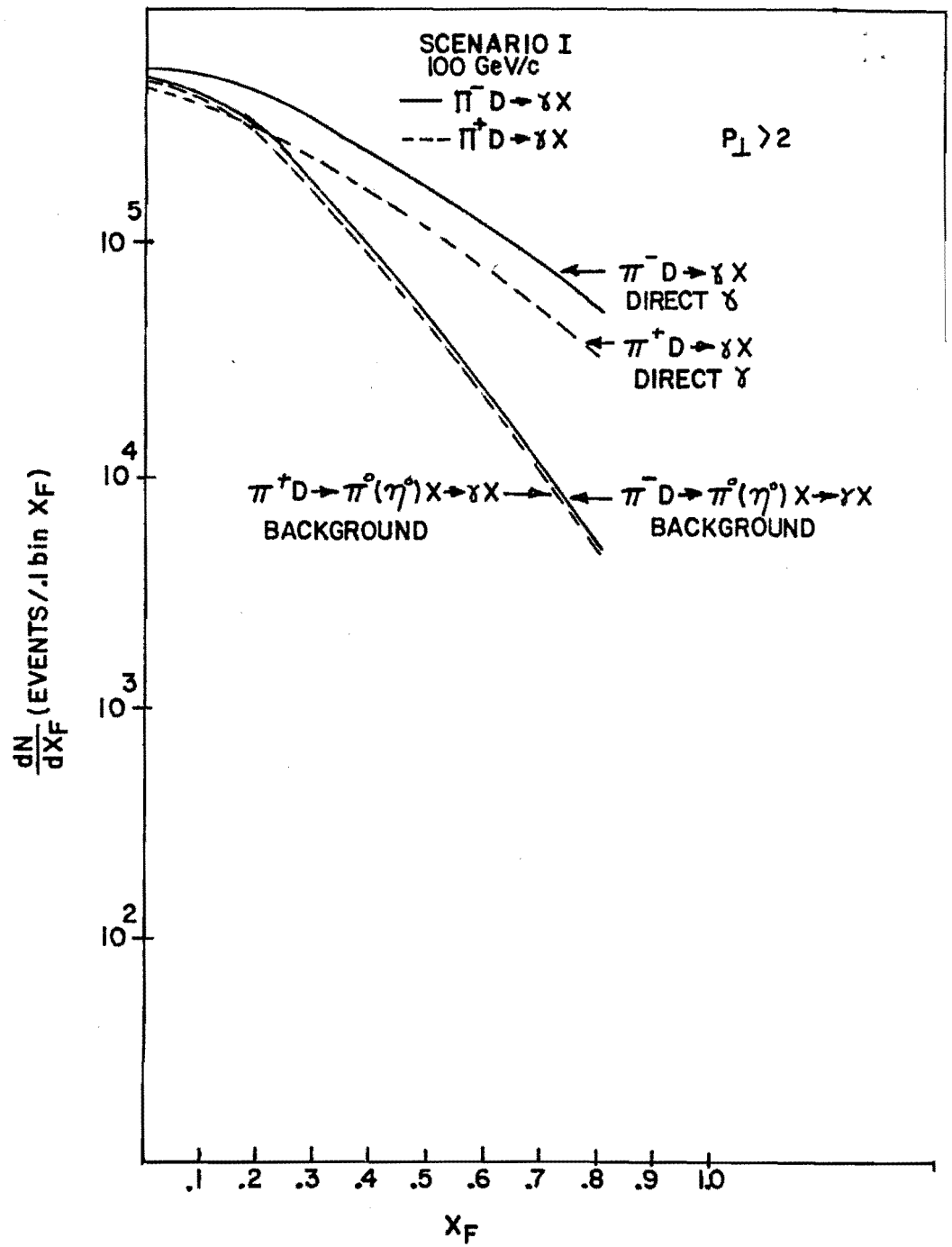

FIGURE 9a

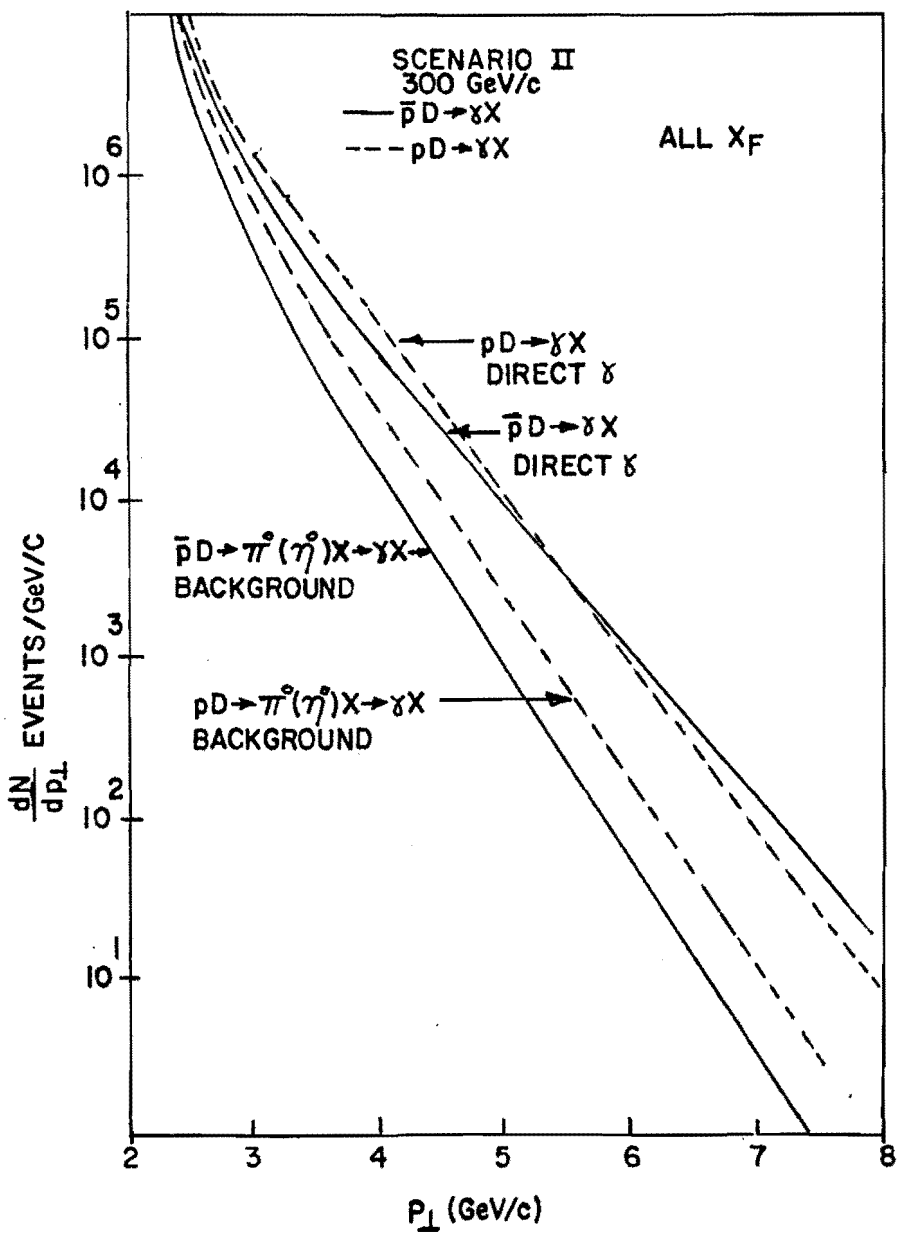

FIGURE 9b

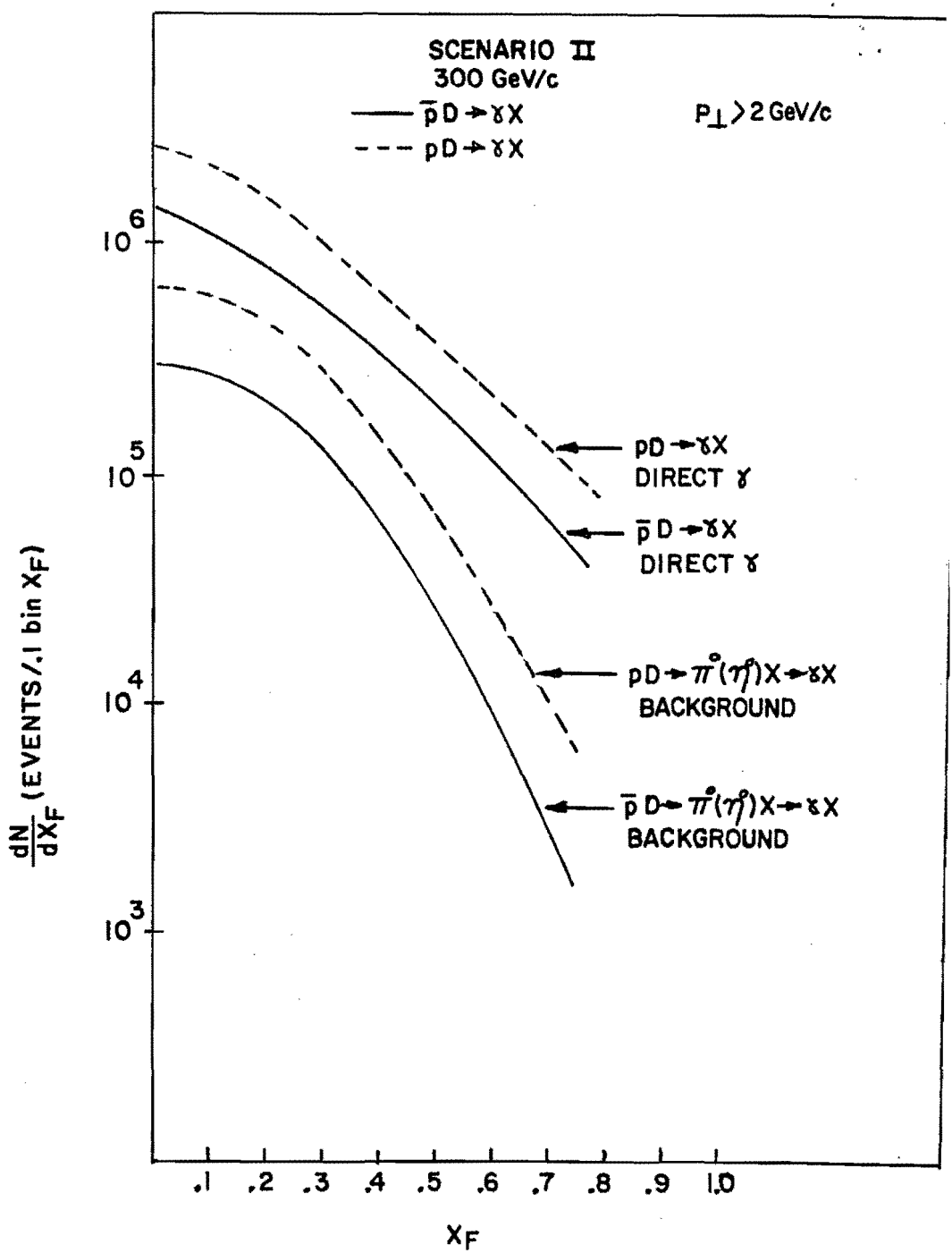

FIGURE 10a

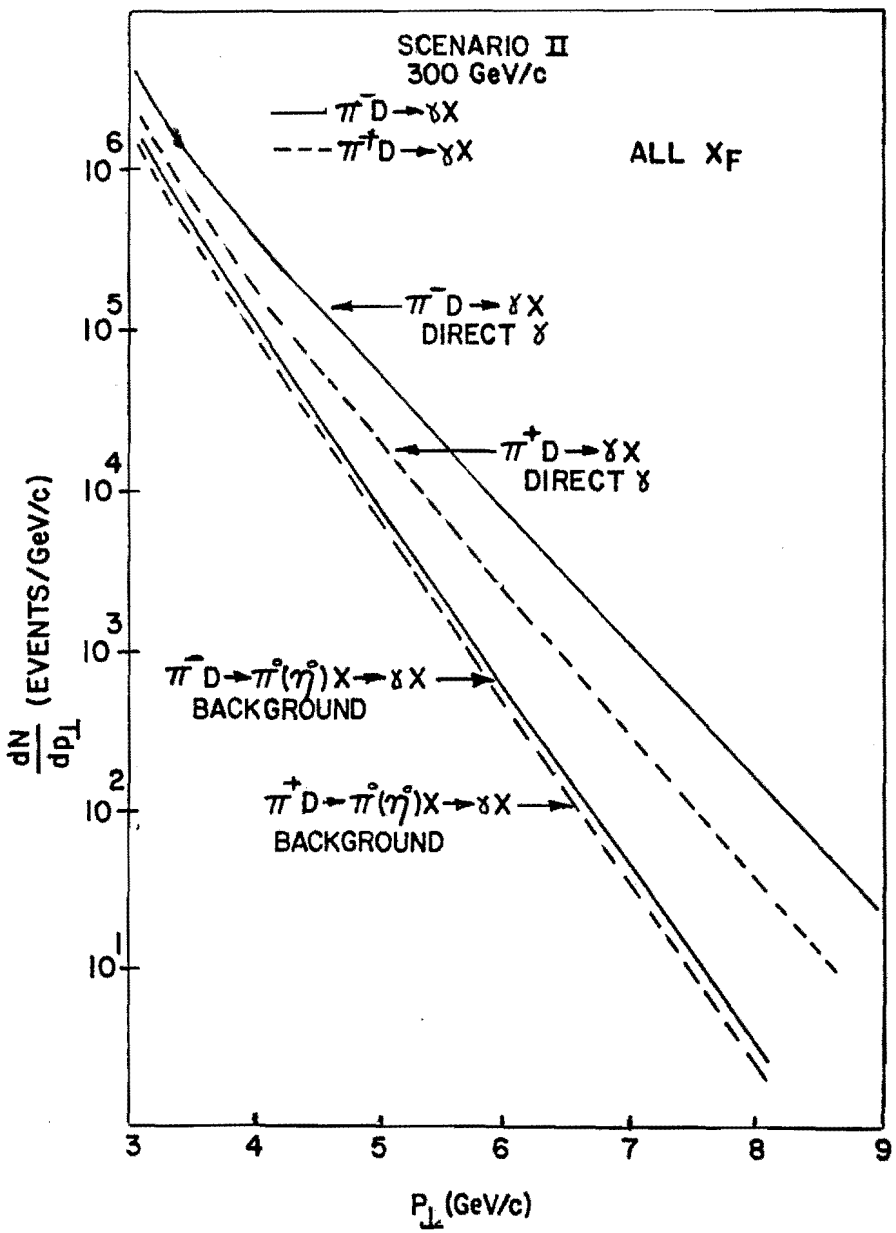

FIGURE 10b

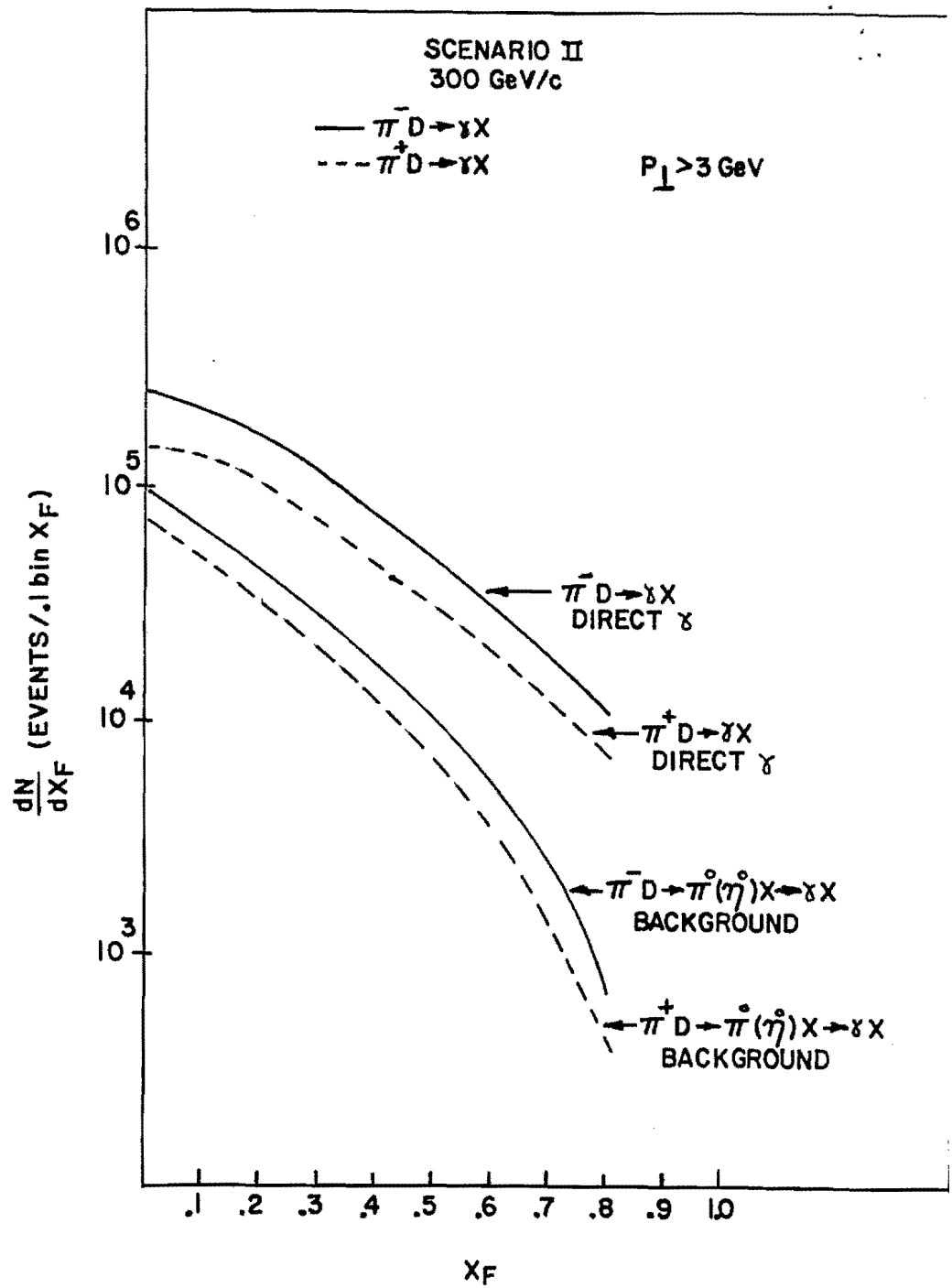

FIGURE 11a

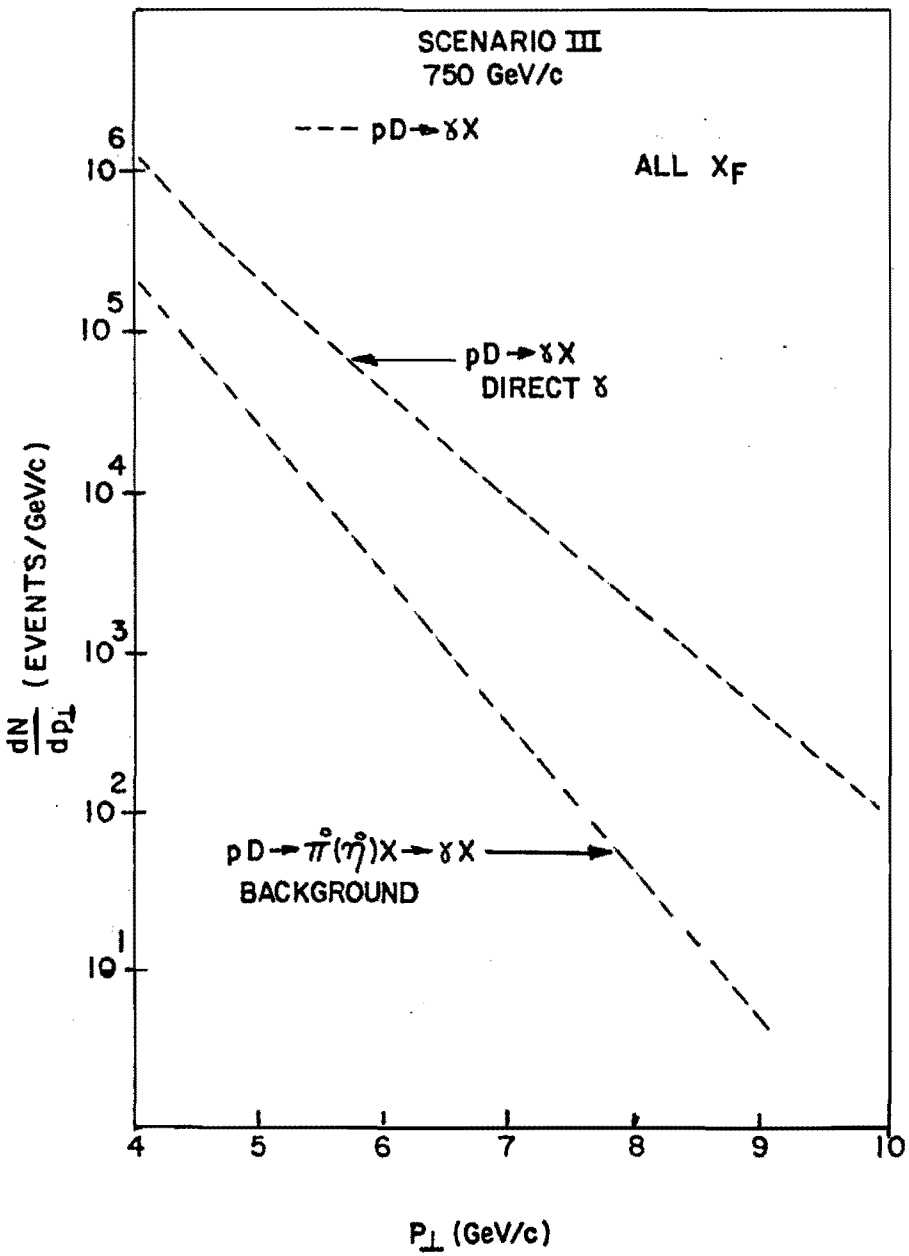

FIGURE 11b

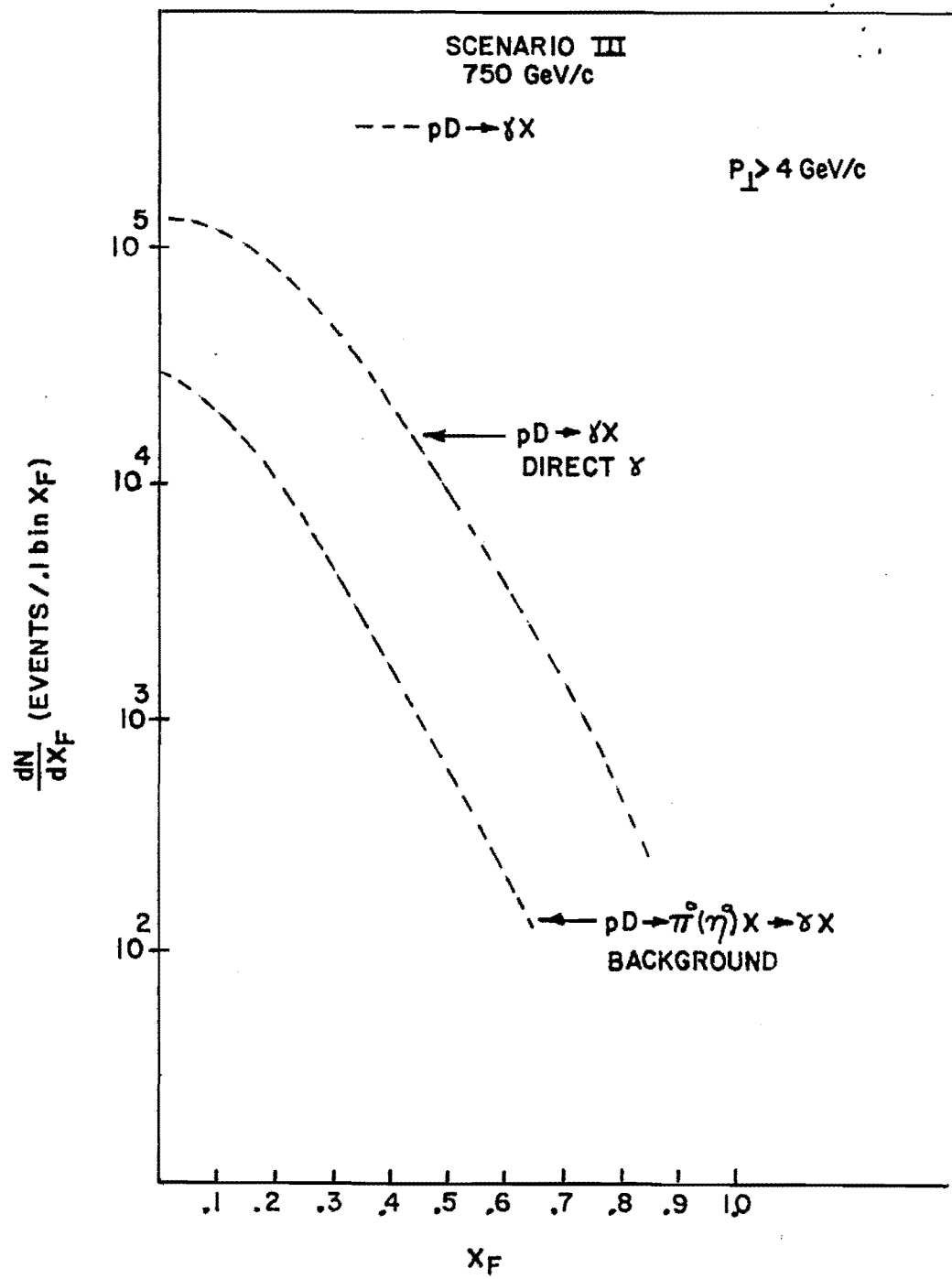

FIGURE 12a

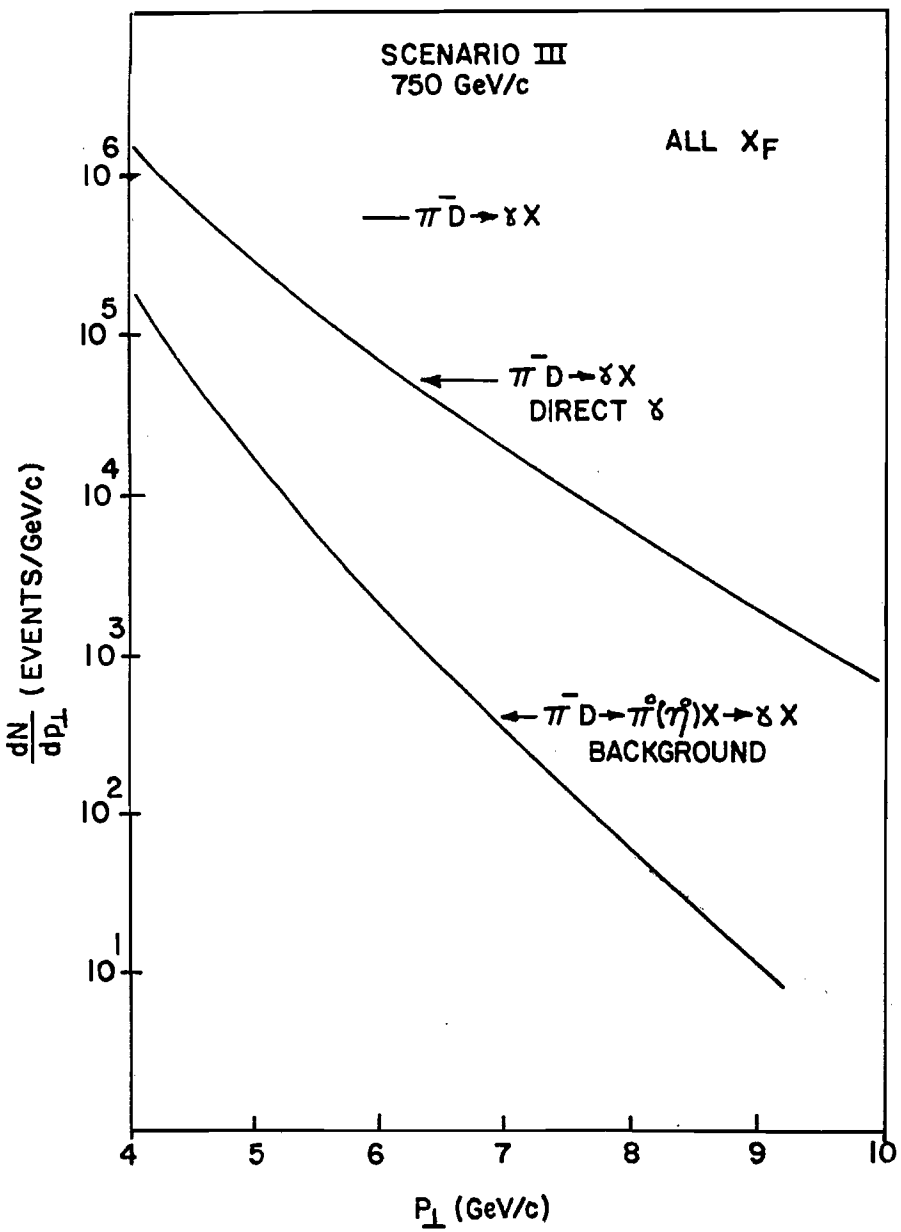

FIGURE 12b

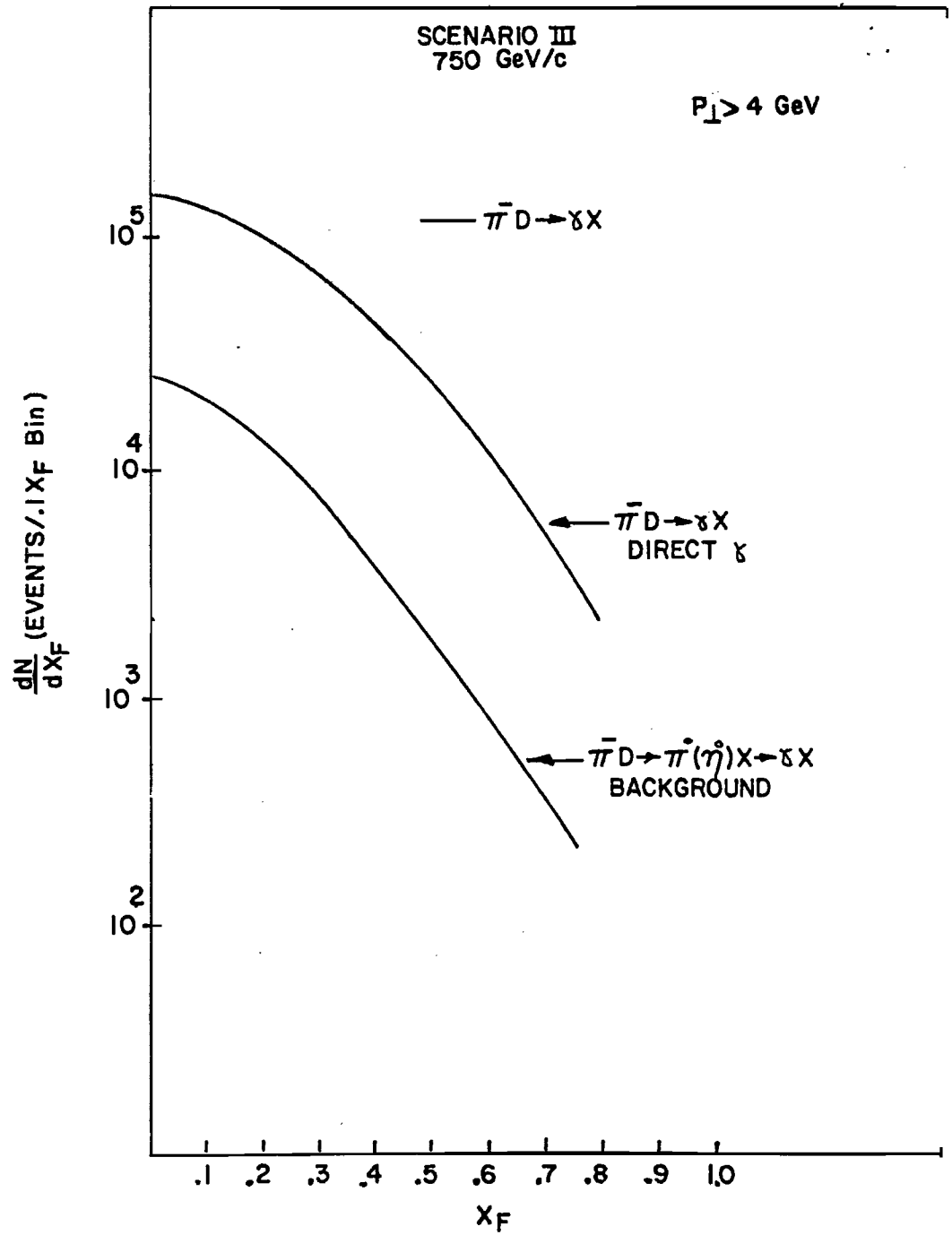

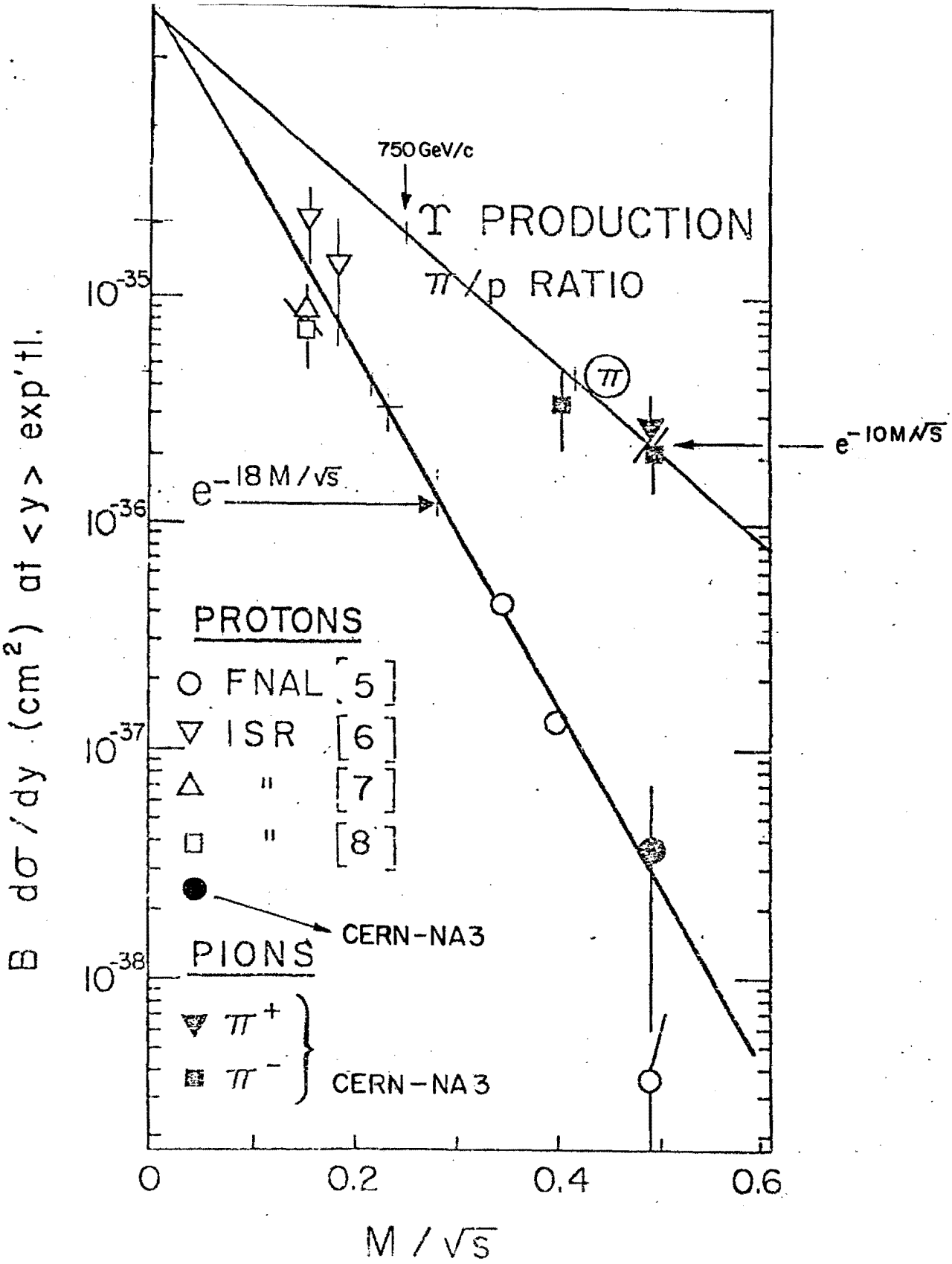

Cross section comparison between protons and pions for Υ production.

FIGURE 14a

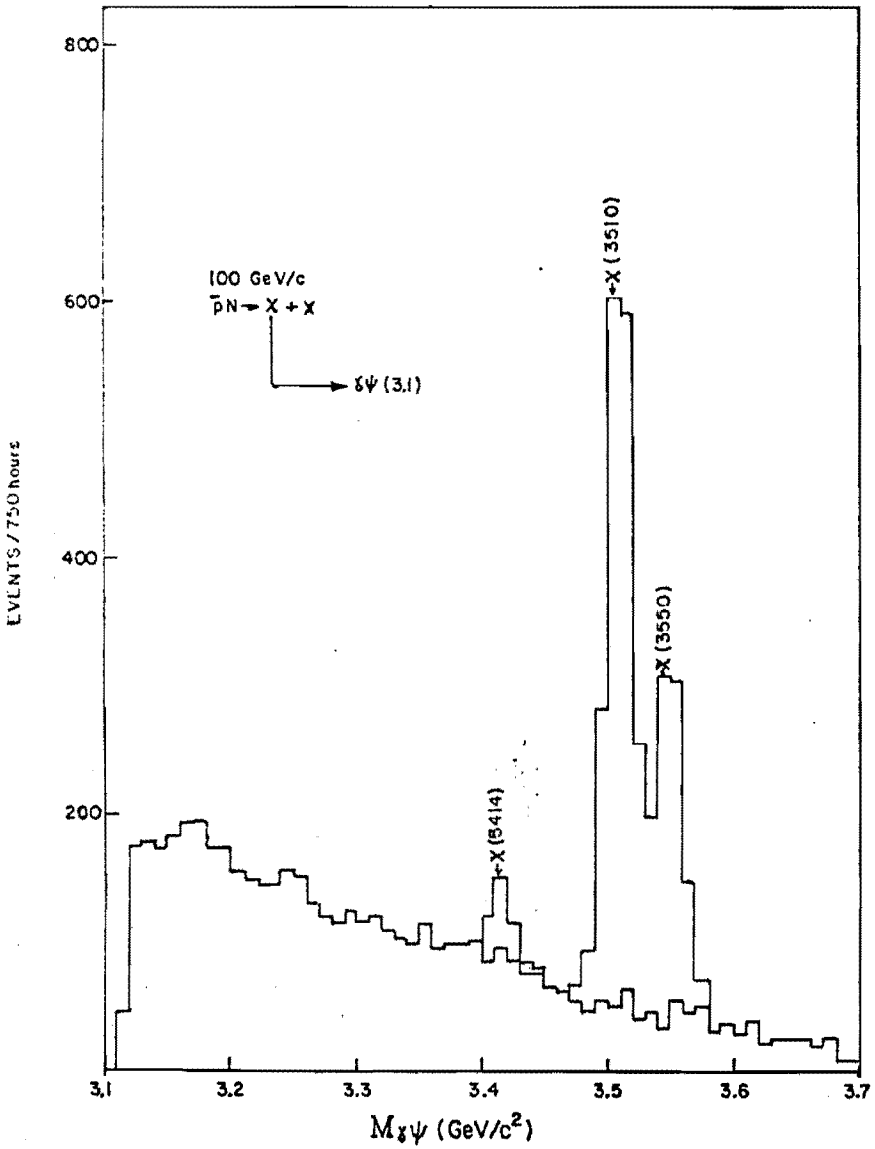

FIGURE 14b

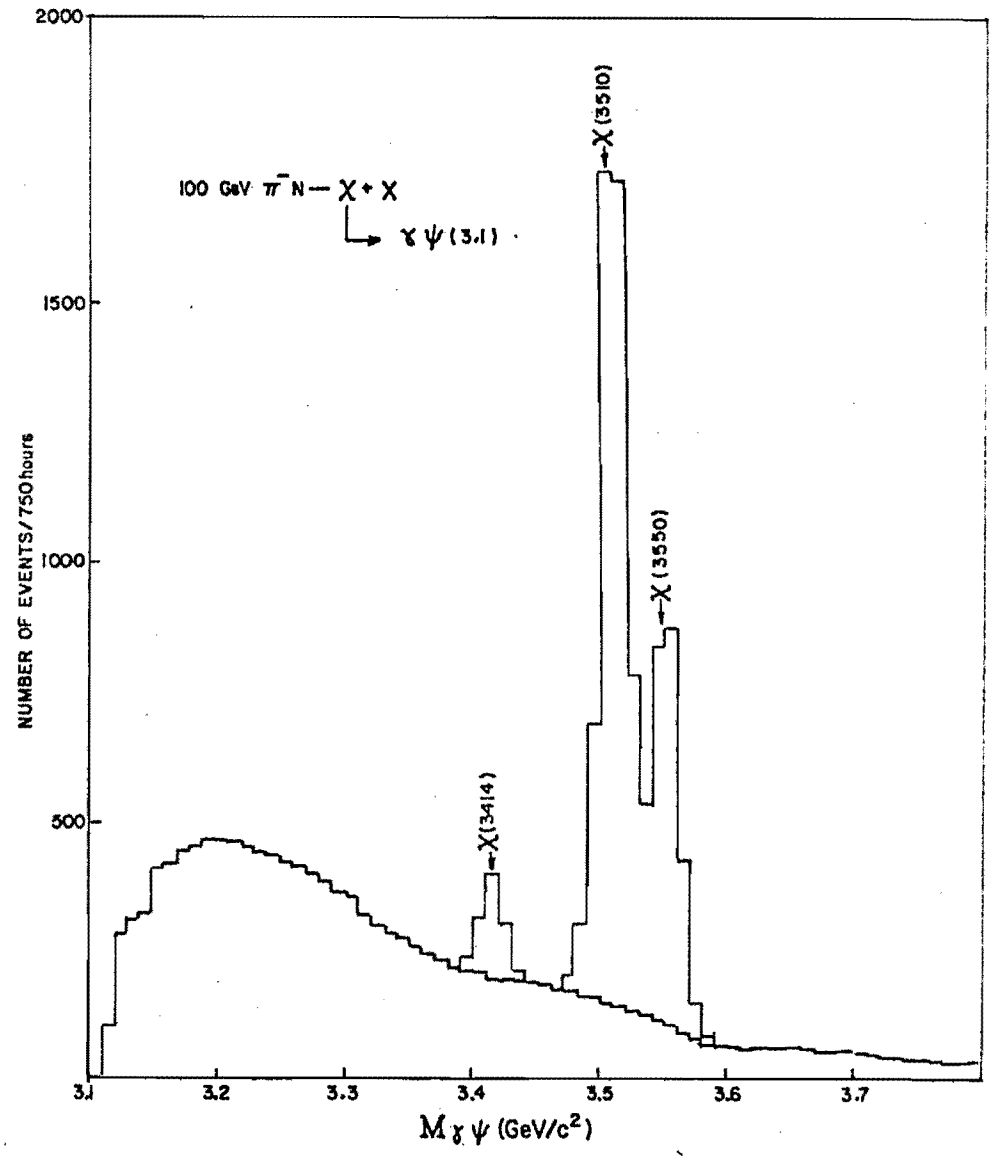

APPENDIX A

E-537 Liquid Argon

Detector

The electromagnetic shower detector which we propose to add to the E-537 spectrometer is a liquid argon detector with the cellular structure shown below:

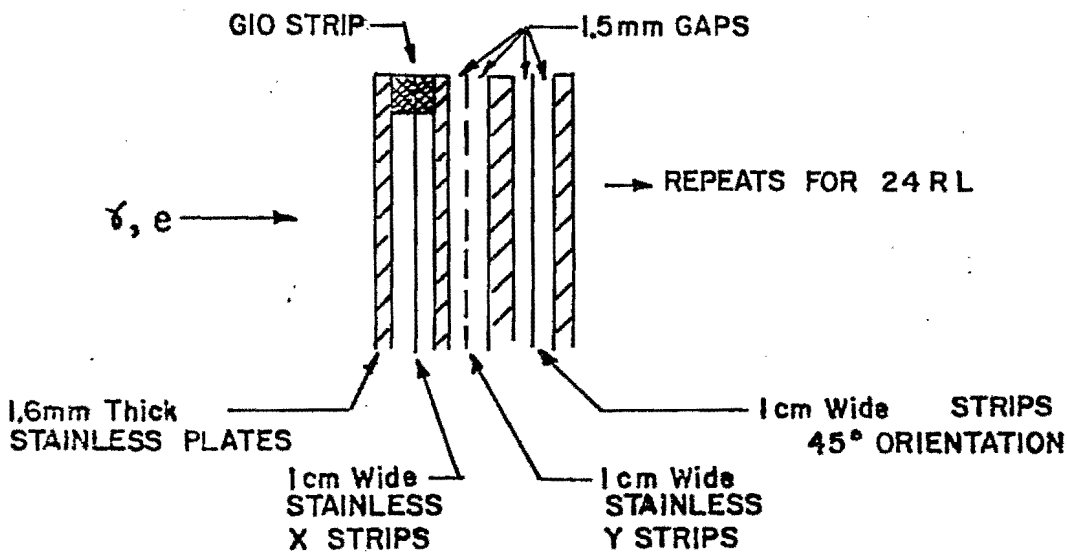

The basic parameters of the device are:

Strip width -	1cm (X,Y), 1.41cm (U/V)
Strip material -	stainless steel
HV plate thickness -	1.6mm
HV plate material -	stainless steel
Liquid argon gap -	1.5mm
HV plate size -	2 meters x 2 meters (Detector consists of two separate identical halves 2m x 2m each.)
Number of plates -	220
U/V angle -	45°
Mass of detector -	26 tons
Volume of L.A. -	5000 liters (7.8 tons)
Size of detector -	4m x 2m x 2m
Cryostat -	foam + stainless steel inner liner
% Methane -	1%

The basic design goals are:

Resolution -	$\sigma \sim 6\% . \sqrt{E}$
Speed (electron collection) -	$\sigma \sim 150$nsec
Anticipated Noise Level -	$\sim$minimum ionizing = 130 MeV

The electronics (suitably modified to meet the trigger needs of the experiment) which we propose to use with this device have been developed by T. Droege of Research Services.[43] The two pulse resolution of this system is of order 150 nsec and 2400 channels are required to instrument the detector.

We expect to be able to construct this device over a period of 1-1.5 years. We have estimated the technician effort to be the equivalent of the construction effort for the E-537 drift chamber system (of order 6 technician years).

APPENDIX B

Cerenkov Counters for Charged Particle Identification

We propose to add three segmented Cerenkov counters C1, C2, and C3 to the E-537 spectrometer as indicated in Figure 1. The elevation and plan views are shown below.

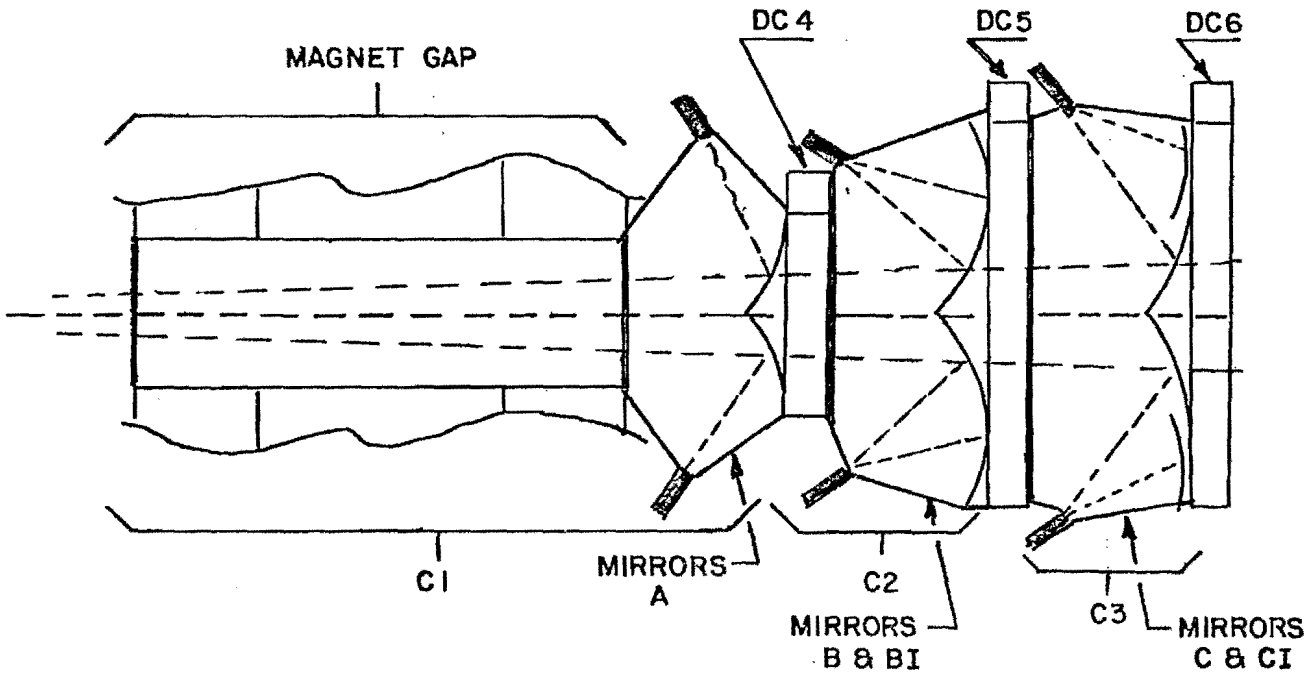

ELEVATION

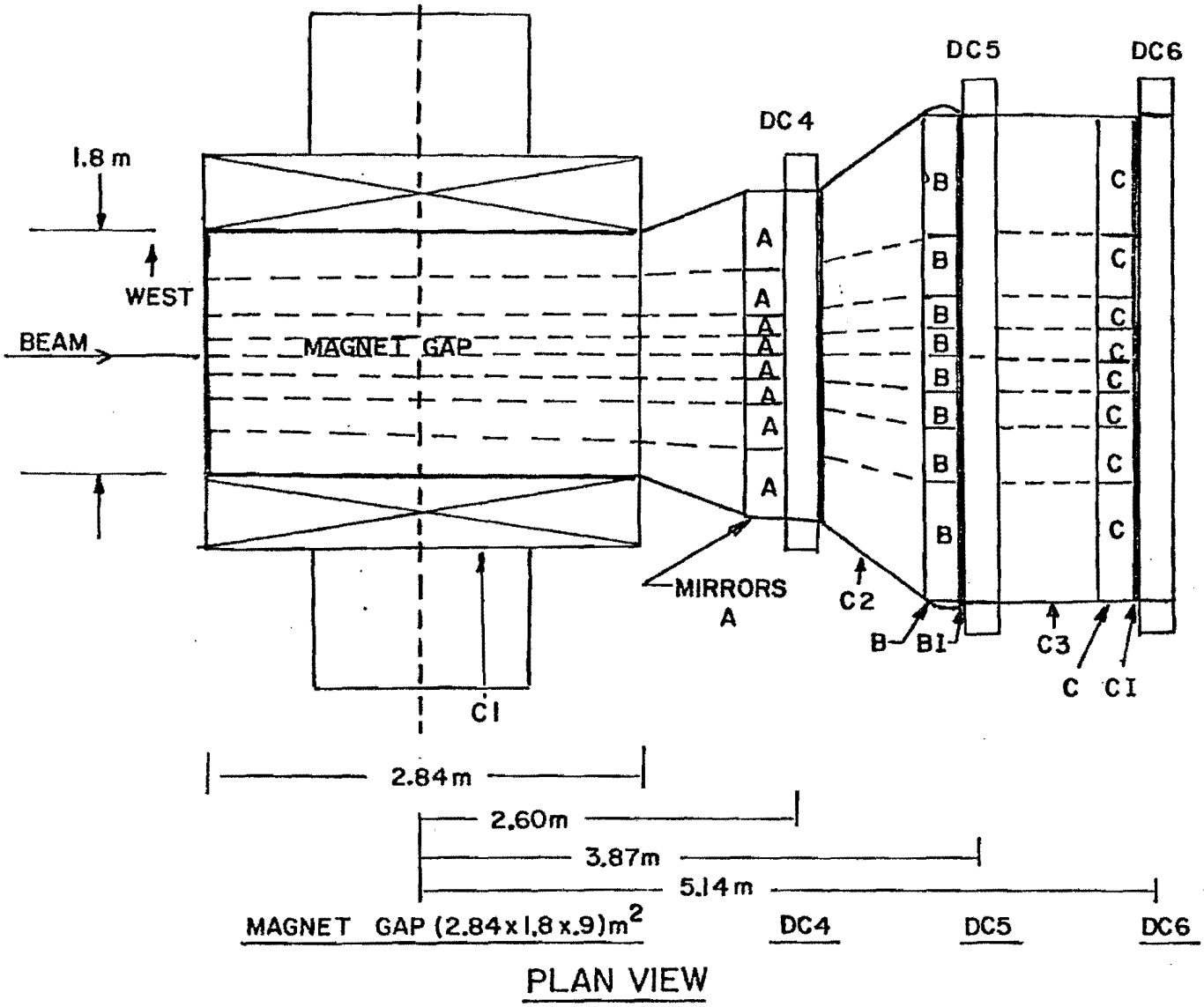

PLAN VIEW

The three Cerenkov counters have 16 cells each and cover the entire solid angle. The cell sizes have been adjusted so that the rate has been equalized in each cell. The mirrors are made out of 2mm aluminized plexiglass reinforced with honeycomb material[44] which contributes less than .005 of a radiation length. The total amount of material contributed by the three Cerenkov counters should be less than .04 of a radiation length. This is to be compared to the average radiation length of D_2 (.065RL) that the photons pass through.

The parameters of each individual counter are given in Table B1.

Table B1

Cerenkov Parameters

		C1	C2	C3
Gas		Ne(He)	Nitrogen	Freon
Refractive Index		1.000063	1.000287	1.000727
Integrated Photons/m (2200-5500A^{o})		15	71	180
Threshold (GeV/c)	π	17	5.6	3.2
	K	59	20	11
	p	112	38	22
Average number of photo-electrons 0.5 GeV/c above threshold*	π	6	8	22
	K	5	7	18
	p	5	7	18
Length (Meters)		4	1.2	1.2
Radiation Length (gas+mirrow+wall)		0.01	0.006	0.02

*These numbers were calculated assuming a photon collection efficiency of 80% and a photocathode quantum efficiency of 20%.

APPENDIX C

Current Results from E-537 Phase I

The basic E-537 spectrometer has been successfully operated for a brief period of time in a closed geometry configuration in order to accumulate data from the reaction

$$\bar{p}N \rightarrow \mu^+\mu^- + X$$

The basic equipment which was used is the same as that shown in Figure 1 with the exception of the new items, the liquid argon detector and the Cerenkov counters which we described in Appendices A and B and with a 60" copper absorber to shield the spectrometer from hadrons from the target. The preliminary data presented in this Appendix represents less than one week of data taking at greatly reduced beam intensities. However this small data sample (less than 0.1% of the data expected from Phase I) is adequate to demonstrate the excellent performance of the basic spectrometer. We expect to complete a major data run for E-537 Phase I before June, 1981.

We show in Figure C1 a typical time distribution and position resolution for our drift chamber system. As shown we are achieving $\sim$200 micron resolutions in these large devices. This gives the expected good mass resolution of $\sigma \sim 4\%$ for the $\psi(3.1)$ shown in Figure C2. This mass resolution is completely dominated by multiple scattering in the copper absorber. If we investigate the angular distributions (specifically the Gottfried-Jackson angle) as a function of dilepton mass we see the expected change from an isotropic distribution in the ψ mass region to a $1+\cos^2\theta$ distribution for events above 4 GeV/c^2.

This feature is shown in Figure C3. We show in Figure C4 the X_F and $P_\perp$ distributions of ψ's produced by the 100 GeV/c π^- and $\bar{p}$. For comparison we show the $P_\perp$ distribution measured by Pilcher and Smith[46] for ψ's produced in 225 GeV/c π^- N interactions. Finally we quote the very preliminary result for the ratio

$$\frac{\sigma(\bar{p}N\to\psi+X)}{\sigma(\pi^-N\to\psi+X)} = 2.5\pm0.8 \qquad X_F>0$$

at 100 GeV/c.

These data represent the first preliminary results for the E-537 spectrometer. We expect to continue this experimentation with greatly increased beam intensities in March, April and May of this year (1981) and to complete this phase of E-537 in the fall of the year.

E-537 DRIFT CHAMBER
PERFORMANCE

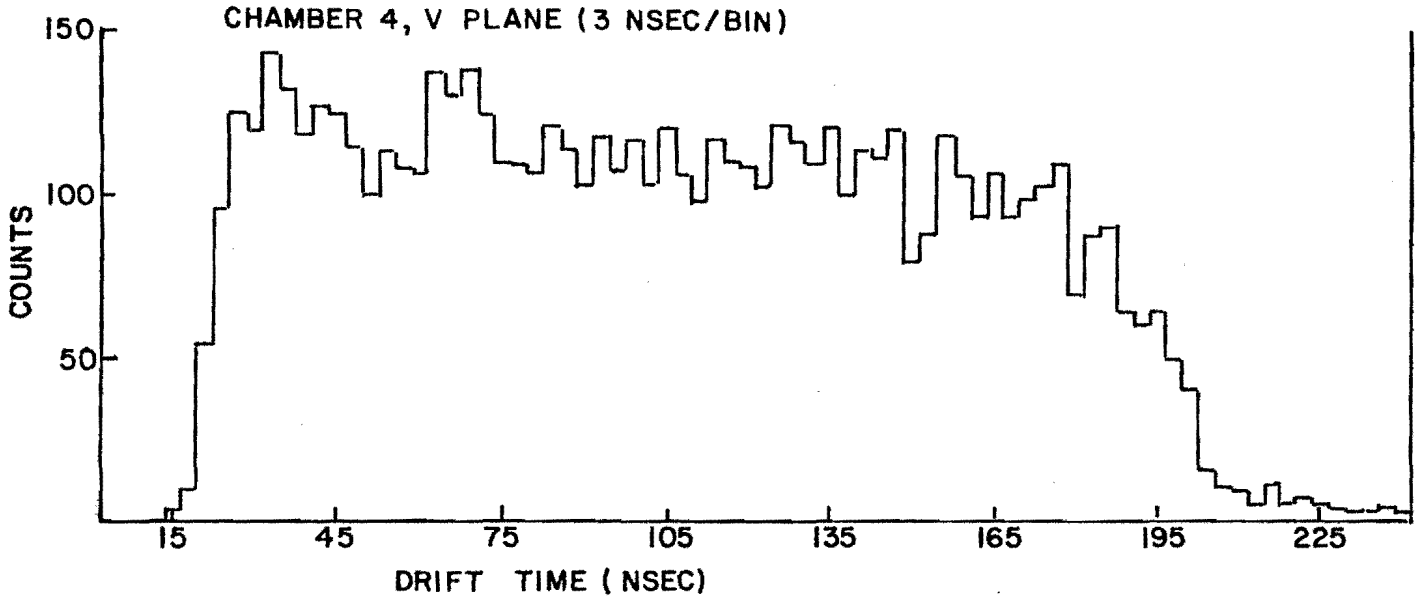

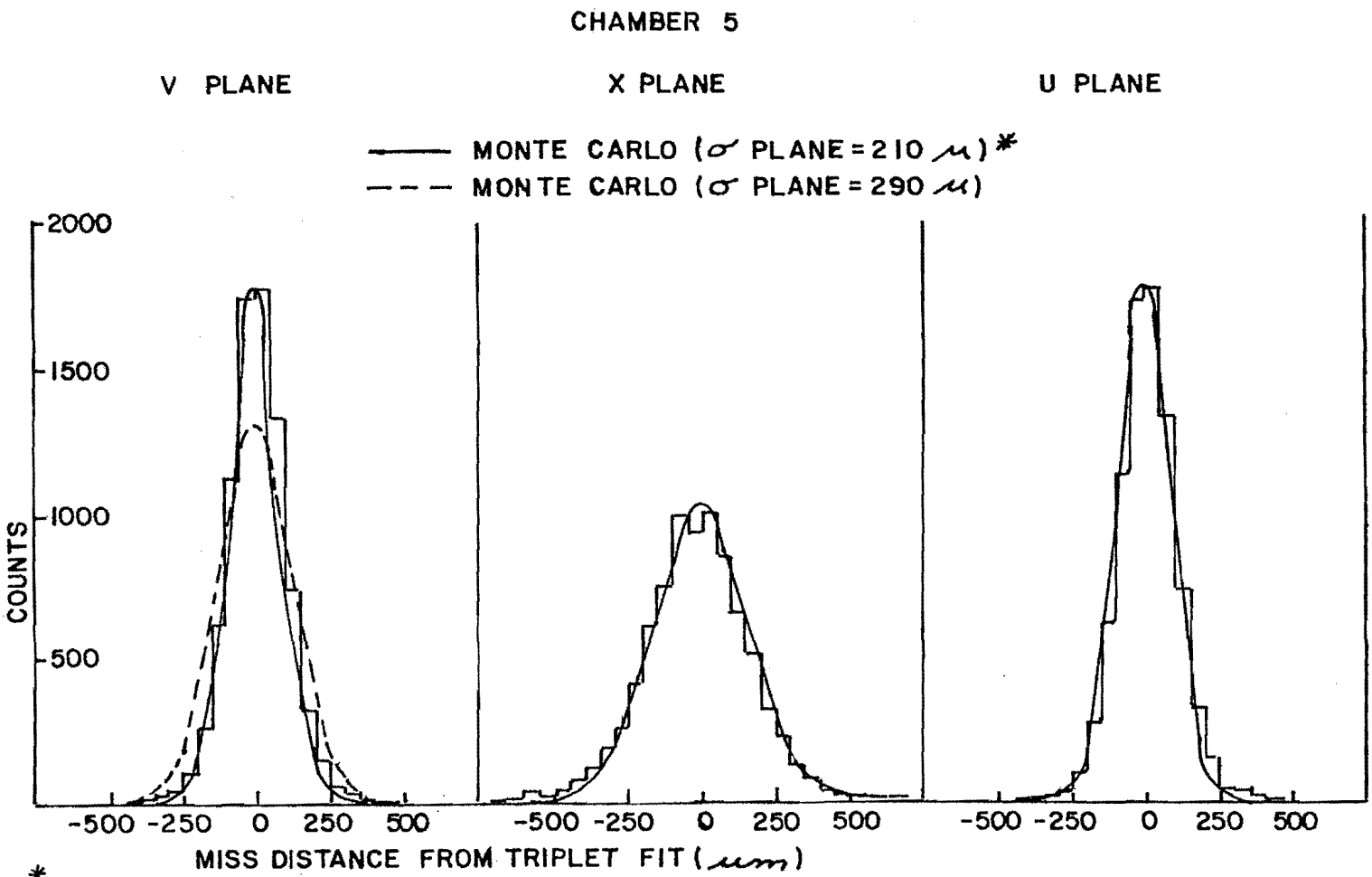

*CURVES SHOW SMALLER WIDTHS THAN σ PLANE BECAUSE ALL PLANES ARE USED IN THE FIT

FIGURE C1

FIGURE C2

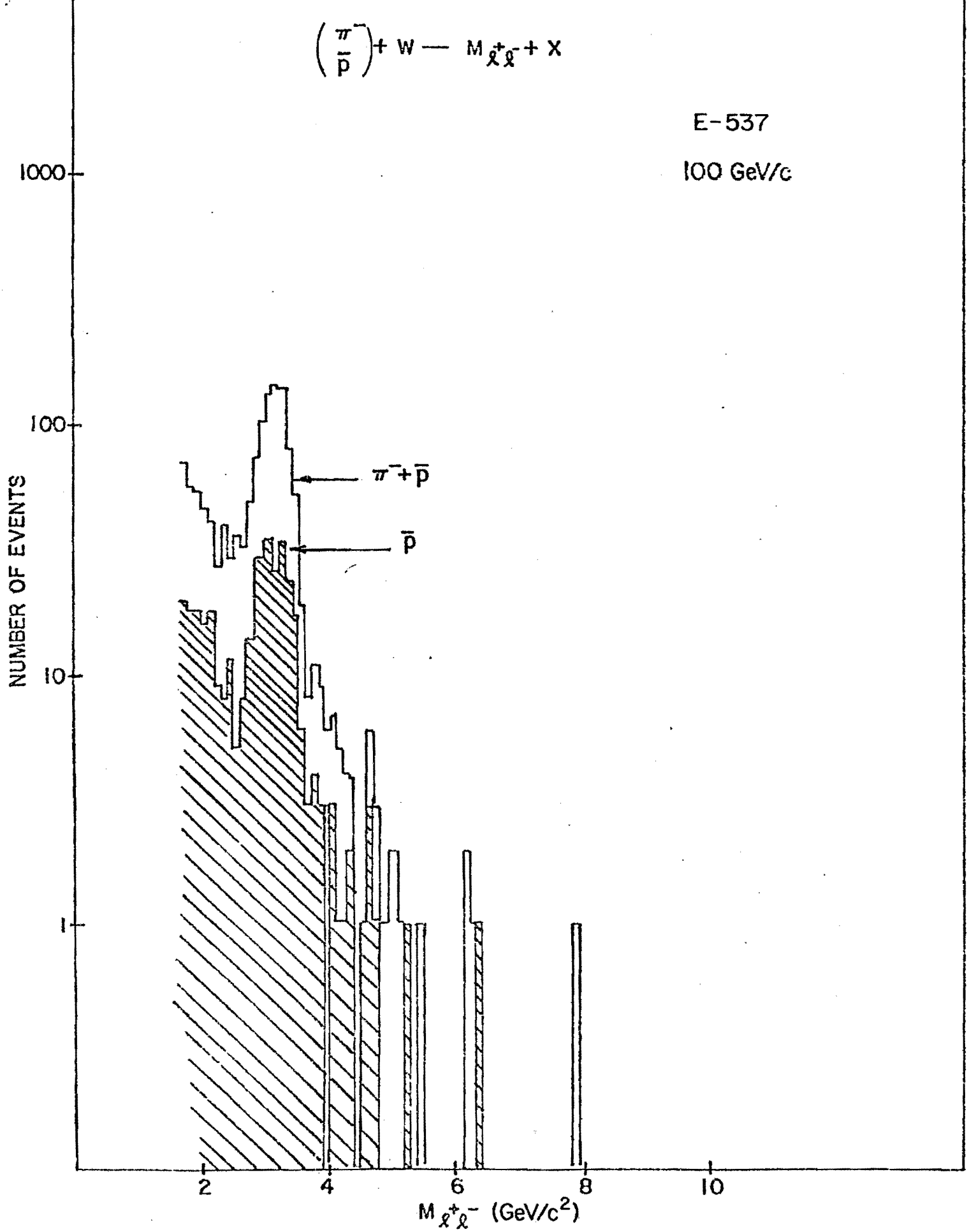
$\left(\frac{\pi^-}{\bar{p}}\right) + W \rightarrow M_{\ell^+\ell^-} + X$
E-537
100 GeV/c
1000
100
10
1
NUMBER OF EVENTS
$\pi^- + \bar{p}$
$\bar{p}$
2
4
6
8
10
$M_{\ell^+\ell^-}$ (GeV/c^2)

FIGURE C3

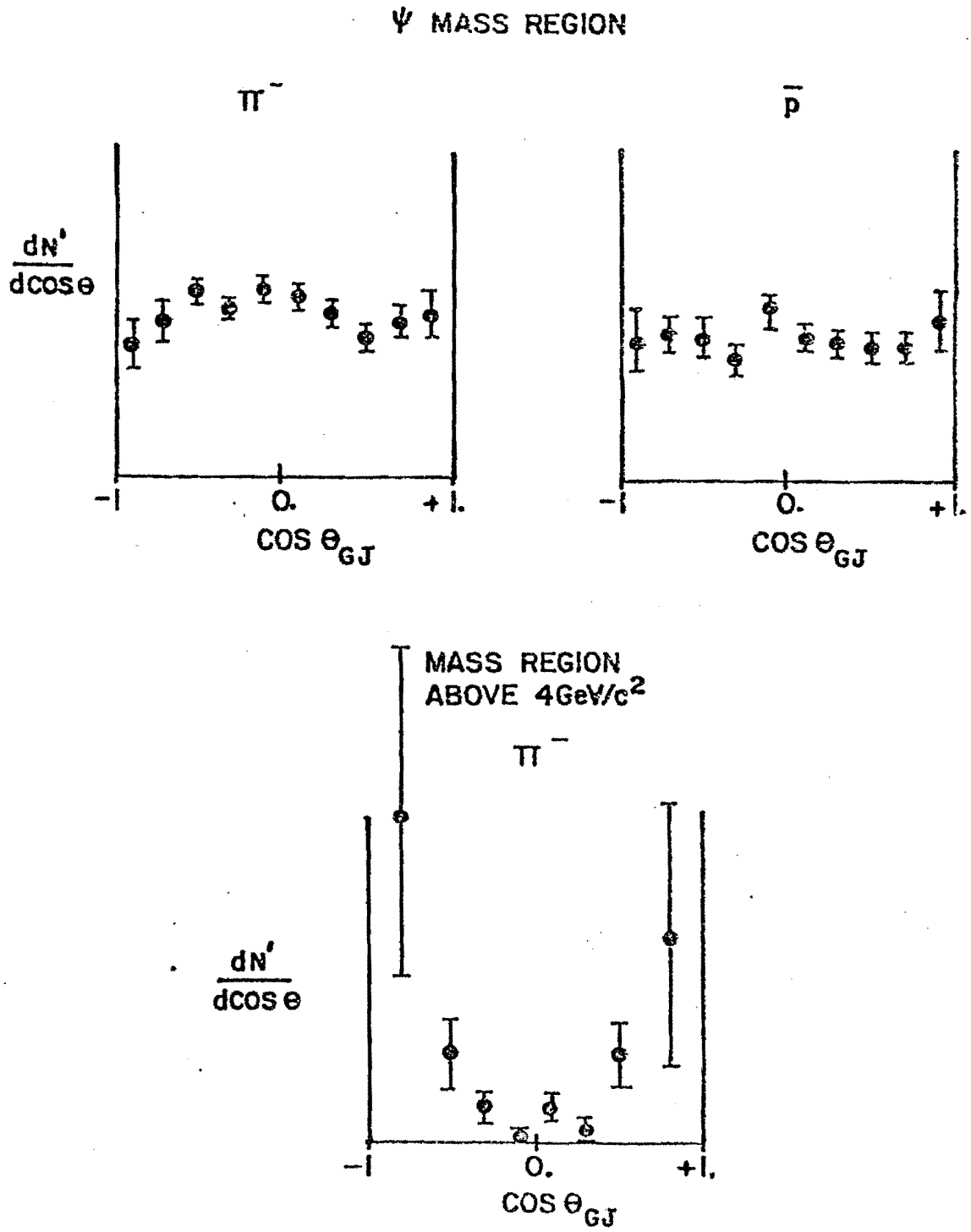
Ψ MASS REGION
π⁻
p̄
dN'/dcosθ
-1
0.
+1.
COS θGJ
MASS REGION
ABOVE 4GeV/c²
π⁻
dN'/dcosθ
-1
0.
+1.
COS θGJ

FIGURE C4a

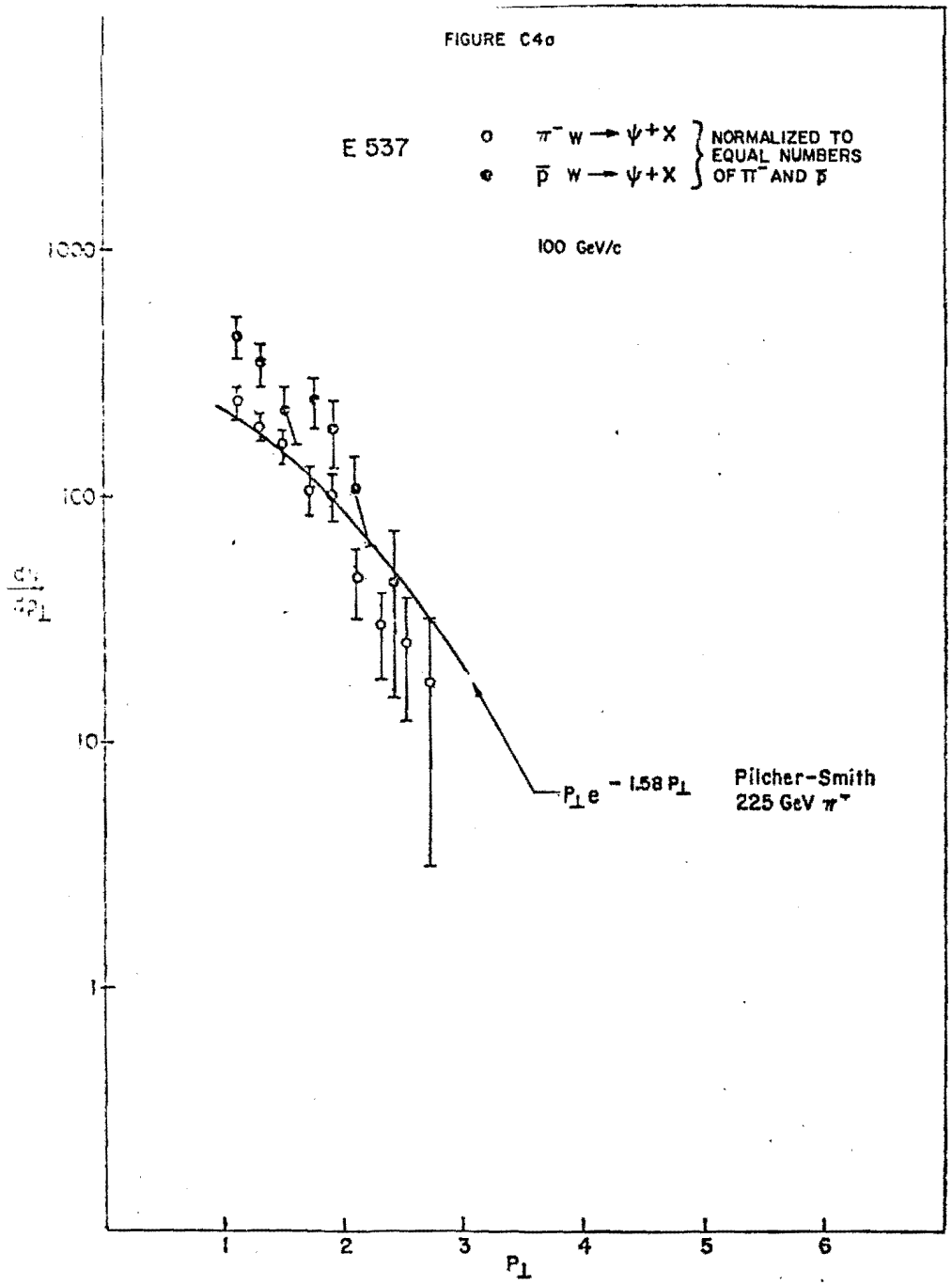
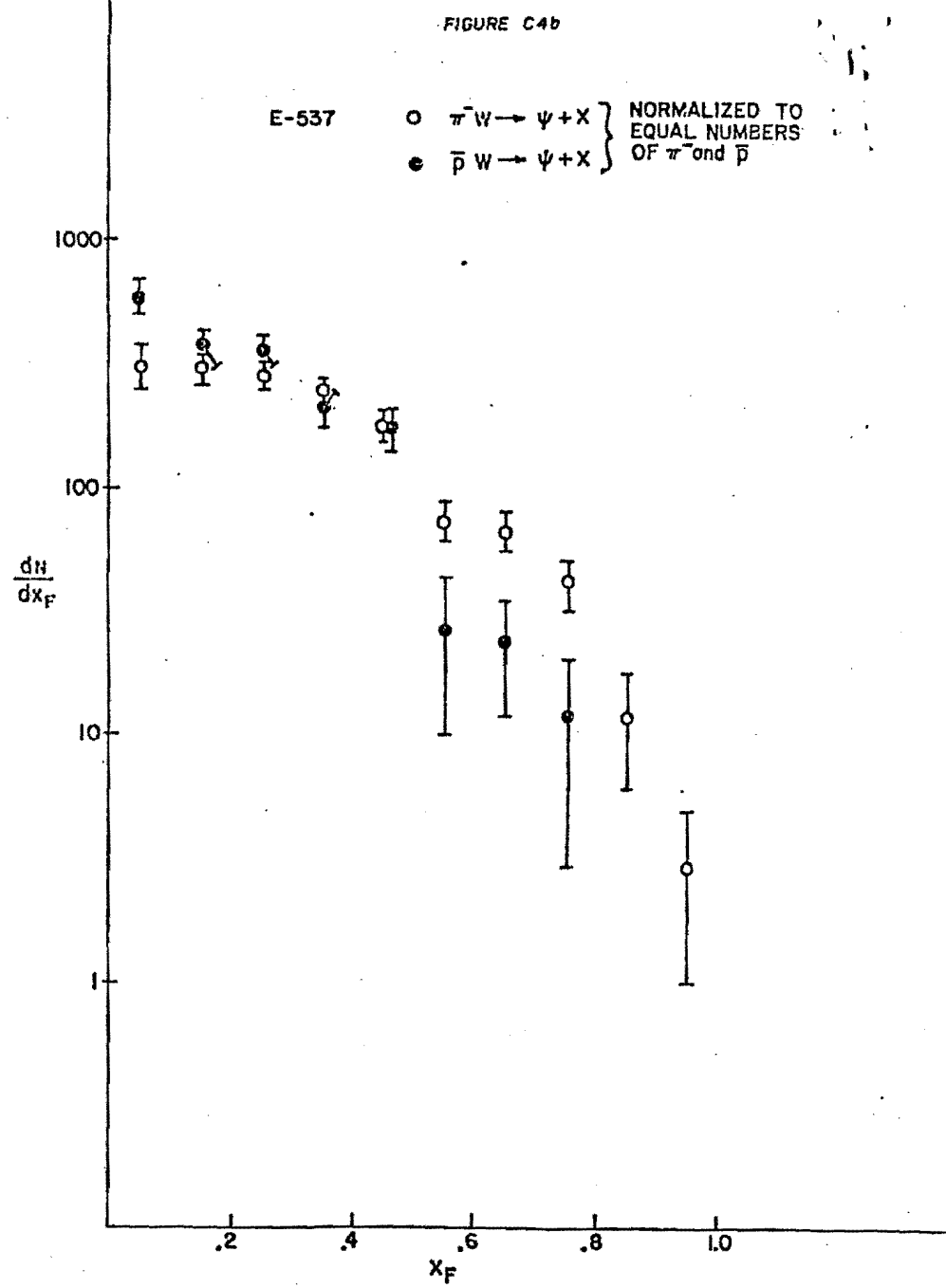
FIGURE C4b